

GPO PRICE \$ \_\_\_\_\_

CSFTI PRICE(S) \$ \_\_\_\_\_

Hard copy (HC) \$3.00

Microfiche (MF) .25

ff 653 July 65

**N 65-35354**

FACILITY FORM 802

(ACCESSION NUMBER)

91

(PAGES)

CR-67299

(NASA CR OR TMX OR AD NUMBER)

(THRU)

(CODE)

(CATEGORY)

**JET PROPULSION LABORATORY  
CALIFORNIA INSTITUTE OF TECHNOLOGY  
PASADENA, CALIFORNIA**

Quarterly Progress Report - 13 May to 13 August 1965

HIGH-PERFORMANCE THERMIONIC CONVERTER

Prepared for:

Jet Propulsion Laboratory  
California Institute of Technology  
4800 Oak Grove Drive  
Pasadena, California

Attention: Mr. Jack L. Flatley, Contract Negotiator

Contract 951225 *under NAS 7-100*

EOS Report 6952-Q-1

23 August 1965

Prepared by:

A. E. Campbell *AEC*

D. H. Pollock *D.H.*

Approved

*for A. O. Jensen*

A. O. Jensen, Manager  
SPECIAL TUBE DEPARTMENT

Approved

*George R. White*

George R. White, Manager  
OPTICAL-ELECTRONICS DIVISION

ELECTRO-OPTICAL SYSTEMS, INC. - PASADENA, CALIFORNIA  
A Subsidiary of Xerox Corporation

## CONTENTS

1.	INTRODUCTION	1-1
1.1	Program Goals	1-1
1.2	Summary of Work Performed	1-2
1.2.1	Variable Parameter Test Vehicle	1-2
1.2.2	Converter Studies	1-2
1.3	Summary of Significant Results and Conclusions	1-4
1.3.1	Radiator Heat Rejection Studies	1-4
1.3.2	Collector Heat Transfer	1-5
1.3.3	High Temperature Brazing	1-5
2.	ELECTRODE MATERIALS EVALUATION	2-1
2.1	Variable Parameter Test Vehicle	2-1
2.1.1	Vehicle Design	2-1
2.1.2	Vehicle Fabrication	2-22
2.1.3	Parametric Measurements	2-26
2.2	Materials Process Study	2-26
2.2.1	Analysis of Stock	2-29
2.2.2	Sample Preparation	2-29
2.2.3	Vacuum Outgassing Schedules for Tantalum	2-32
2.2.4	Surface Stability Examination	2-32
3.	COLLECTOR STUDY AND SECONDARY EXPERIMENTS	3-1
3.1	Collector Heat Transfer Study	3-1
3.1.1	Thermal Design Curves for Non-Composite Collector	3-1
3.1.2	Composite Collector Thermal Experiment and Metallographic Analyses	3-4
3.2	Radiator Heat Rejection	3-7
3.2.1	Rokide "C" Investigation	3-7
3.2.2	Radiator Fin Analysis	3-18
3.2.3	Non-Integral Collector-Radiator	3-24

## CONTENTS (contd.)

3.3 Converter Fabrication Investigation	3-27
3.3.1 High-Temperature Brazing	3-27
3.3.2 Heater-Wire End Seals	3-28
3.3.3 Converter Seal-Off	3-32
3.3.4 Ceramic-Metal Seals	3-35
3.3.5 Interelectrode Spacing	3-38
4. CONVERTER DESIGN	4-1
5. PROGRAM FOR NEXT QUARTER	5-1
5.1 Variable Parameter Test Vehicle	5-1
5.2 Emitter Materials Process Study	5-1
5.3 Non-Integral Collector Radiator	5-1
5.4 Composite and Non-Composite Collector Experiments	5-1
5.5 Converter Fabrication Investigations	5-1
5.6 Converter Design	5-2
REFERENCES	
APPENDIX A - PROCEDURE FOR CHEMICAL CLEANING OF TANTALUM	A-1

## ILLUSTRATIONS

2-1	Variable Parameter Test Vehicle	2-3
2-2	Setup for Collector Heat Transfer Experiment	2-9
2-3	Idealized Collector-Radiator System	2-10
2-4	Collector Surface Temperature as a Function of Collector Current Density (Calculated)	2-12
2-5	Collector Isotherm Distribution	2-14
2-6	Guard Ring Isotherm Distribution	2-15
2-7	Interelectrode Potential Distributions	2-16
2-8	Drive Mechanism Layout	2-18
2-9	Support Structure Layout	2-20
2-10	Emission Vehicle Layout	2-24
2-11	Emission Vehicle Test Schematic	2-27
2-12	Constant Current-Voltage Sweep Load	2-28
2-13a	Tantalum Process Sample Vacuum-Fired at 2100°C for 2 Hours in a Vac-Ion Pumped Atmosphere of $1 \times 10^{-7}$ torr	2-33
2-13b	Same Sample after Operation at 1735°C for 100 Hours at $5 \times 10^{-8}$ torr	2-33
2-14a	Tantalum Process Sample Vacuum-Fired at 2250°C for 2 Hours in a Vac-Ion Pumped Environment of $4 \times 10^{-7}$ torr	2-34
2-14b	Same Sample after Operation at 1735°C for 100 Hours in a Vac-Ion Pumped Environment of $5 \times 10^{-8}$ torr	2-34
3-1	Thermal Design Curves for Noncomposite Collector	3-3
3-2	Composite Collector, Molybdenum and Copper	3-5
3-3a	Micrograph of Molybdenum-Copper Interface	3-6
3-3b	Micrograph of Molybdenum-Copper Interface Nearest Collector Surface	3-6
3-4	Thermocouple Locations and Sample Dimensions of Molybdenum-Rokide "C" Experiment	3-8
3-5	Rokide "C"-Coated Molybdenum Sample after 500 Hours of Operation	3-10

# ILLUSTRATIONS (contd)

3-6	Cooldown Curves of Rokide "C"-Coated Molybdenum Sample	3-13
3-7	Cooldown Curves of Rokide-Coated Copper Sample	3-17
3-8	Elemental Forms of Converter Radiators	3-19
3-9	Model for Constant-Temperature-Gradient Fin Analysis	3-20
3-10	Nonintegral Collector-Radiator Assembly	3-26
3-11	Vanadium Overbrazed at 2150°C of Rhenium to Niobium	3-29
3-12	Detail of Overbrazed Vanadium-Rhenium Interface	3-30
3-13	Vanadium Braze at 1900°C of Rhenium to Niobium	3-31
3-14	End Connection for Sheathed Heater Wire	3-33
3-15	Marginal Pinchoff of Copper Tubing Reservoir	3-34
3-16	Satisfactory Pinchoff of Copper Tubing Sample	3-36
3-17	Thermal Environment Oven for Ceramic-Metal Seal Testing	3-37
3-18	Setup for Measuring Interelectrode Spacings in a Mockup Converter	3-39

## 1. INTRODUCTION

This is the first quarterly report of progress on J.P.L. Contract 951225, a program to (1) investigate basic materials, processes, and operating parameters affecting the stability and optimization of cesium vapor thermionic converters, and (2) to apply the results of these investigations to the fabrication of practical, high performance, high efficiency, long life cesium vapor thermionic converters.

### 1.1 Program Goals

The program goals are: (1) to generate fundamental data on the various operational parameters such as interelectrode spacing, Langmuir-Taylor type cesiated electron emission and work function of various electrode materials, and to establish optimum electrode materials processing, all to be applicable to practical cesium vapor thermionic converters. (2) Conduct auxiliary experiments pertinent to the engineering design and converter fabrication in a manner such that the results are applicable to practical, high efficiency, long life cesium vapor thermionic converters, and (3) design, fabricate, and test a maximum of six cesium vapor thermionic converters utilizing the results of the auxiliary experiments, leading to a performance of 20 watts/cm<sup>2</sup> at 0.8 volts output and an efficiency exceeding 14% for an emitter temperature of 1735°C.

Adequate attention will be accorded the collector and radiator heat transfer problems so that a practical converter with a 2 cm<sup>2</sup> emitter having an output of 40 watts at 0.8 volts can be fabricated with a minimum radiator weight. The weight of the converters must be consistent with the achievement of a four-converter generator weighing less than

four pounds. The radiator area of the converters must be such that no additional cooling (such as excessive thermal conduction down the collector lead straps) is necessary for operation of the converter at its design conditions.

## 1.2 Summary of Work Performed

### 1.2.1 Variable Parameter Test Vehicle

#### 1.2.1.1 Design

The design of the variable parameter test vehicle has been completed and approved by J.P.L.

#### 1.2.1.2 Fabrication

The fabrication of the variable parameter test vehicle has been initiated.

#### 1.2.1.3 Electrode Materials Processing Study

The establishment of processing schedules for the electrode materials to be used in the variable parameter emission test vehicle has been approximately one half completed. The processing schedule for tantalum bar stock has been examined and that for rhenium plate stock is in process.

### 1.2.2 Converter Studies

#### 1.2.2.1 Auxiliary Experiments

##### 1.2.2.1.1 Collector Heat Transfer

Heat transfer experiments and metallurgical examinations have been made on a molybdenum collector with solid copper inserts and on a stepped molybdenum collector in pursuit of reducing by conventional methods the thermionic converter collector barrel temperature drop at high heat load ( $150\text{-}200\text{ watts/cm}^2$ ). An analysis of collector  $\Delta T$  as a function of the thermal power density, with length to cross-sectional area ratios as a parameter, has been completed.

#### 1.2.2.1.2 Radiator Heat Rejection Studies

Long term experiments pertaining to the effective emissivity and stability of Rokide C coatings on molybdenum and copper radiators operating at 600°C have been completed.

A first order optimized radiator fin analysis has been completed for the flat fin radiator.

Brazing, and initial heat transfer experiments have been completed on a molybdenum collector -- flat copper radiator composite.

#### 1.2.2.1.3 Ceramic to Metal Seal Studies

Materials have been obtained for metal to ceramic seal studies involving thick niobium (.020" to .040") flanges. The test apparatus, including a rapid response vacuum oven and thermal cycling control, for the evaluation of thick metal member seal assemblies under thermal shock conditions has been completed. These studies are being pursued in an effort to arrive at more compact converter designs.

#### 1.2.2.1.4 Converter Seal-Off Studies

Comparison of various copper tubulation pinch off tools has been completed.

#### 1.2.2.1.5 Heater Wire End Seal

A simple direct method has been developed for the attachment of rugged, thermally efficient, end seals to clad heaters of the Ta-Al<sub>2</sub>O<sub>3</sub>-Ta type. These heaters are used on the converter cesium reservoir and radiator for parametric optimization

#### 1.2.2.1.6 Interelectrode Spacing Studies

The design of the experiment for the direct observation and measurement of interelectrode spacing variation as a function of emitter and collector temperature has been completed.

#### 1.2.2.1.7 Electron Beam Welding

Experiments to establish a reliable electron beam welding schedule for rhenium to rhenium joints have been completed. The metallurgical examination of the process samples is in progress.

#### 1.2.2.1.8 High Temperature Brazing

Preliminary studies of rhenium to niobium braze joints utilizing a vanadium braze shim have been completed.

### 1.3 Summary of Significant Results and Conclusions

#### 1.3.1 Radiator Heat Rejection Studies

##### 1.3.1.1 Rokide Coating Stability

Rokide "C" coatings of nominally .002" thickness on molybdenum and copper have been found to be absolutely stable at 600°C for times in excess of 500 hours. The effective value of the emissivity has been determined to be 0.78 in comparison to handbook values of 0.85 to 0.9. The effective emissivity of these coatings at 600°C does not change for coating thickness between .002" and .006". No peeling, chipping, degradation or evaporation of these coatings was observed over the 500 hour test. The results apply to both the molybdenum and copper substrates at a temperature of 600°C in a  $10^{-7}$  mm Hg ion-pumped environment.

##### 1.3.1.2 Composite Radiator-Collector

A copper radiator-molybdenum collector composite has been fabricated and tested in a preliminary fashion. The initial tests are indicating that this scheme is a factor of 2 better than molybdenum on a heat rejection per unit weight basis. The composite radiator-collector retains the mechanical strength features of the integral molybdenum collector-radiator for generator mounting purposes.

### 1.3.2 Collector Heat Transfer

A molybdenum collector with copper inserts has been successfully fabricated and tested under thermal cycling conditions. This composite is calculated to improve the effective thermal conductivity of the molybdenum collector barrel by 30 percent.

### 1.3.3 High Temperature Brazing

Rhenium-niobium braze joints utilizing vanadium as the braze material do not exhibit the presence of any brittle inter-metallic compounds when the correct braze schedule is employed. The joint appears ductile.

## 2. ELECTRODE MATERIALS EVALUATION

### 2.1 Variable Parameter Test Vehicle

A variable parameter vehicle has been designed for great versatility in measurements over the wide range of parameters necessary to characterize electrode material performance for application to thermionic energy converters. The device is capable of obtaining both cesiated and vacuum electron emission measurements on a variety of electrode materials. In addition, power output measurements, as a function of spacing, can be performed with electrode temperatures at optimum.

The major portion of the first quarter effort on the variable parameter test vehicle has been applied to the development of the basic vehicle design and a complete thermal analysis of this design. Test vehicle instrumentation and power supply requirements have been studied, an automatic electronic load has been designed, and its assembly is complete. The availability of an electronic load will reduce data accumulation time and increase the accuracy and validity of the emission measurements.

#### 2.1.1 Vehicle Design

Before a detailed design and thermal analysis of a variable parameter test vehicle could begin, a basic decision concerning temperature measurement was required. A design which allowed the accurate determination of emitter (cathode) temperatures had to be selected. Due to the high temperature instability of thermocouple measurements during long term operation (a result of material diffusion at the bi-metal junction), a pyrometer method of measurement, utilizing an 8 to 1 blackbody hole was chosen. Since the largest contribution to measurement inaccuracy in this method is extraneous radiation, a device geometry

was selected which allowed an unobstructed view of the blackbody hole by a micro-optical pyrometer.

Based on these considerations, the design geometry utilizes a concentric guard ring and a collector barrel with exposed emitter. Figure 2-1 shows the geometry of the vehicle. An added benefit of this design is the ability to eliminate all possibility of a parasitic cesium reservoir.

The length of the collector barrel is determined by both heat transfer considerations and, mechanically, the fact that it must be coaxial with a guard ring of a particular length. The length of the guard ring is mainly set by the mechanical limitations which are introduced by the requirement that the guard ring-collector move with respect to the emitter and emitter envelope.

#### 2.1.1.1 Variable Parameter Test Vehicle Thermal Analysis

A primary consideration in the thermal design of the emission vehicle was to provide equal temperature distributions (zero contact potential) along the guard ring and collector barrel and, at the same time, minimize the collector barrel length to reduce  $\Delta T$  in the collector barrel at high heat fluxes.

To determine whether the guard ring and collector have equal or nearly equal thermal gradients and hence zero contact potential difference since they are fabricated of the same material, consider the following derivation. The heat conducted down the collector barrel is

$$Q_{\text{coll}} = k_{\text{coll}} A_{\text{coll}} \left. \frac{dT}{dx} \right|_{\text{coll}}, \quad (1)$$

where  $Q_{\text{coll}}$  is the heat flux conducted down the collector,  $k_{\text{coll}}$  is the thermal conductivity of the collector material,  $A_{\text{coll}}$  is the cross-sectional area of the conducting path and  $\left. \frac{dT}{dx} \right|_{\text{coll}}$  is the thermal gradient

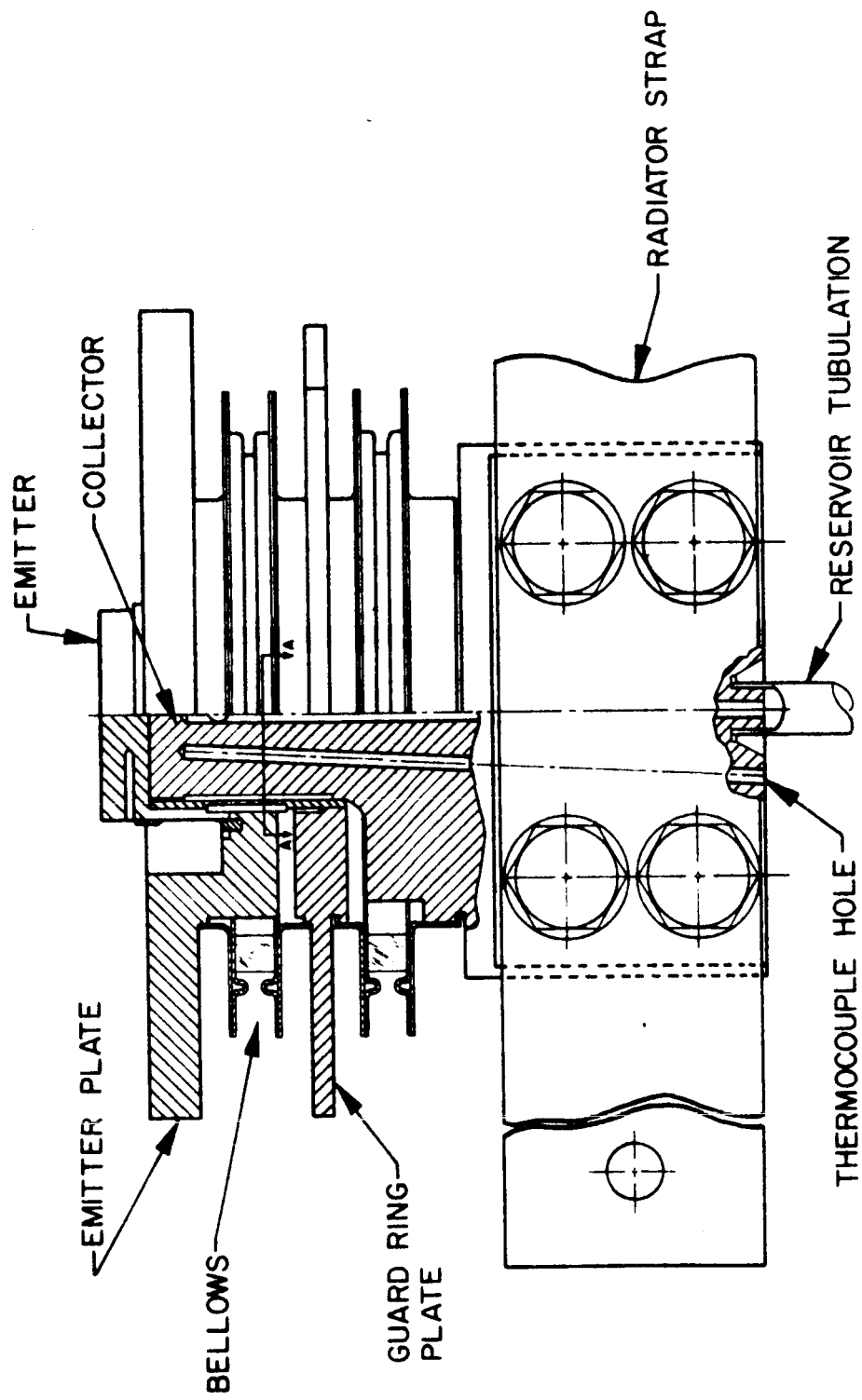


FIG. 2-1 VARIABLE PARAMETER TEST VEHICLE

down its length. The heat conducted down the guard ring is given by

$$Q_{g.r} = k_{g.r} A_{g.r} \left. \frac{dT}{dx} \right|_{g.r} \quad (2)$$

where the quantities in Eq. 2 are the same as in Eq. 1 except that they apply to the guard ring structure. Now, the heat flux input to the collector barrel is

$$Q_{coll} = J \phi_{coll} A_{coll} \quad (3)$$

and the heat flux input to the guard ring is

$$Q_{g.r.} = J \phi_{g.r.} A_{g.r.} \quad (4)$$

where, in both Eqs. 3 and 4,  $J$  is the electron current density emitted by the emitter (cathode),  $\phi_{coll}$  and  $\phi_{g.r.}$  are the effective thermal work functions of the collector and guard ring, and  $A_{coll}$  and  $A_{g.r.}$  are the collector areas for the collector and guard ring, respectively. The effective thermal work function for heat transfer purposes is dependent upon the apparent surface work function  $\phi_c$  (as determined from emission data), the plasma electron energy ( $E_{plasma} = 4kT_{plasma}/\pi e$ ), and the energy gained (or lost) at the accelerating (or retarding) sheath at the collector or guard ring surface. In the condition where the collector is matched to the plasma, there is no sheath at the anode surface and, for heat transfer purposes,

$$\phi_{eff_{th}} = \phi_c + \frac{\epsilon kT_p}{e} \pm V_s \quad \nearrow 0$$

where  $1.3 \leq \epsilon \leq 1.5$  depending on the plasma electron energy distribution.

It is apparent from the foregoing discussion that a heat transfer analysis cannot be valid without consideration of plasma conditions within the interelectrode space. The effect of these

plasma conditions on the thermal power input can be demonstrated by considering the case of a matched plasma at the collector (anode) (i.e., no collector sheath), a plasma electron temperature of 6000°K (a probable maximum condition), and an apparent minimum work function for cesiated molybdenum of 1.55 eV. In this case,  $V_p = 4kT_{\text{plasma}}/e$  is 0.66 eV. This results in  $\phi_{\text{effth}} = 2.21$  eV (for heat transfer purposes), which is a correction of 40 percent to the thermal power input to the collector or guard ring over apparent work function considerations.

Returning to the derivation, since the guard ring and collector are of the same material, the conductivities and work functions are identical, if equal temperatures are assumed. In addition, due to the noncontoured geometry, the collecting area is the same as the cross-sectional area of the conducting path. Therefore, substitution of Eqs. 3 and 4 into Eqs. 1 and 2 yields

$$J \phi_{\text{coll}} = k_{\text{coll}} \left. \frac{dT}{dx} \right|_{\text{coll}} ; J \phi_{\text{g.r.}} = k_{\text{g.r.}} \left. \frac{dT}{dx} \right|_{\text{g.r.}} \quad (5)$$

and, as a result of the fact that the collector and guard ring are identical,

$$k_{\text{coll}} \left. \frac{dT}{dx} \right|_{\text{coll}} = k_{\text{g.r.}} \left. \frac{dT}{dx} \right|_{\text{g.r.}}$$

$$\left. \frac{dT}{dx} \right|_{\text{coll}} = \left. \frac{dT}{dx} \right|_{\text{g.r.}} \quad (6)$$

Thus, the temperature gradients are identical down the guard ring and collector, resulting in equivalent temperature distribution. This produces equal cesiated work functions and thus a zero contact potential difference.

The emitter is supported by the emitter heat choke envelope. This envelope is coaxial with the guard ring and collector and provides the electrical connection between the emitter and

emitter lead straps. The envelope is a critical member of the vehicle which accomplishes three important tasks: (1) it must act as an effective heat choke, thermally isolating an emitter which may operate at temperatures in excess of 1800°C from structural members of the device which should not exceed temperatures of 800°C to 900°C; (2) it must carry currents in excess of 400 amperes without a large voltage drop over the length of the envelope; and (3) it must maintain vacuum and mechanical integrity.

The "optimum" heat choke design requires balancing the electrical losses with the thermal losses. From the following equation, a practical L/A ratio must be obtained which minimizes  $\alpha$ , the ratio of electrical loss to thermal loss.

$$\alpha = \frac{I^2 \rho \frac{L}{A}}{K \Delta T \left( \frac{A}{L} \right) - \frac{1}{2} I^2 \rho \left( \frac{L}{A} \right)}, \quad (7)$$

where I is the total current (in amperes) passing through the heat choke,  $\rho$  is the resistivity of the material, L is the length of the heat choke, A is the cross-sectional area of the heat choke wall, K is the thermal conductivity of the material and  $\Delta T$  is the temperature drop across the heat choke. The terms in the denominator of Eq. 7 are the thermal losses in the envelope. This consists of heat conduction (the first term) and half the joule heating (the second term) due to the possibility of joule losses flowing out either end of the envelope.

Heat choke envelopes of two different materials must be designed, one of rhenium and one of tantalum. The design procedure is to determine practical values of L and A and evaluate  $\Delta T$  from Eq. 7 as a function of the parameter  $\alpha$ . Table 2-I summarizes the results based on this approach. Heat conduction K is evaluated for an average temperature of 1000°C.

TABLE 2-I  
HEAT CHOKE ENVELOPE DESIGN PARAMETERS

	Rhenium	Tantalum
L	0.200 inch	0.150 inch
A	0.005 inch (wall)	0.003 inch (wall)
I	250 amperes	250 amperes
$\rho$	$80 \times 10^{-6} \Omega\text{-cm}$	$60 \times 10^{-6} \Omega\text{-cm}$
K	0.48 watt/cm- $^{\circ}\text{C}$	0.67 watt/cm- $^{\circ}\text{C}$
$\Delta T$	1165 $^{\circ}\text{C}$	1005 $^{\circ}\text{C}$
$\alpha$	0.48	0.48

From the values shown in the table, the thermal power conducted down the rhenium heat choke is 86 watts, the Joule heating power generated in the heat choke is 33 watts, and the power radiated by the envelope is 9 watts. Therefore, the total power lost by the emitter down the rhenium envelope is 62 watts for an emitter temperature of 1700 $^{\circ}\text{C}$  and an emitter current of 250 amperes. For tantalum, the thermal power conducted down the heat choke is 80 watts, the Joule heating power generated in the envelope is 31 watts, and the radiated power is 11 watts. Then the total power drained from the emitter by a tantalum heat choke envelope is 60 watts for an emitter temperature of 1700 $^{\circ}\text{C}$  and an emitter current of 250 amperes.

The method chosen for heat rejection from the collector is the mechanical attachment of a copper water- or air-cooled heat sink. The heat sink consists of 1-inch copper straps, 1/8-inch thick, which are connected to copper bus bars by flexible copper straps. The bus bars have been fitted with copper tubing which can be used for air or water cooling of the bus bars to accomplish a variable thermal conduction. An experiment was conducted to determine the heat transfer characteristics of such a mechanically clamped collector-radiator combination. The experimental arrangement and the position of thermocouples

is shown in Fig. 2-2. The results of a heat transfer experiment on this combination are summarized in Table 2-II.

TABLE 2-II  
BOLTED COLLECTOR RADIATOR HEAT TRANSFER EXPERIMENT  
FOR VARIABLE PARAMETER EMISSION TEST VEHICLE  
Constant Electrical Power Input to Gun: approx. 350 watts  
Collector Surface Temperature: approx. 900°C

Collector Base Temperature	Power Conducted Out Lead Strap	Type of Auxiliary Cooling
617°C	158.3 watts	Flexible leads
608°C	239.2	Flexible leads with air cooling, 20 psi air pressure
603°C	245.6	Flexible leads with H <sub>2</sub> O cooling flow rate of 1 liter/min
593°C	265.3	Flexible leads with H <sub>2</sub> O cooling flow rate of 2 liter/min

The difference between power conducted out lead straps and electrical power input to gun is the power radiated by the gun and the collector. As can be seen from Table 2-II, over 100 watts additional power can be conducted out the collector radiator straps by varying the means of cooling. This results in a 25°C variation of the collector root temperature, which is the more significant result. In addition to controlling the collector root temperature by cooling, heaters have been added to the radiator straps for maintaining the collector temperature at desirable levels at low currents. To determine the collector root temperature as a function of heater power, consider the idealized system shown in Fig. 2-3. In the illustration,  $Q$  is the thermal power into the collector,  $1/2 Q$  is the thermal power out each radiator strap assuming no radiation losses,  $q$  is the heater

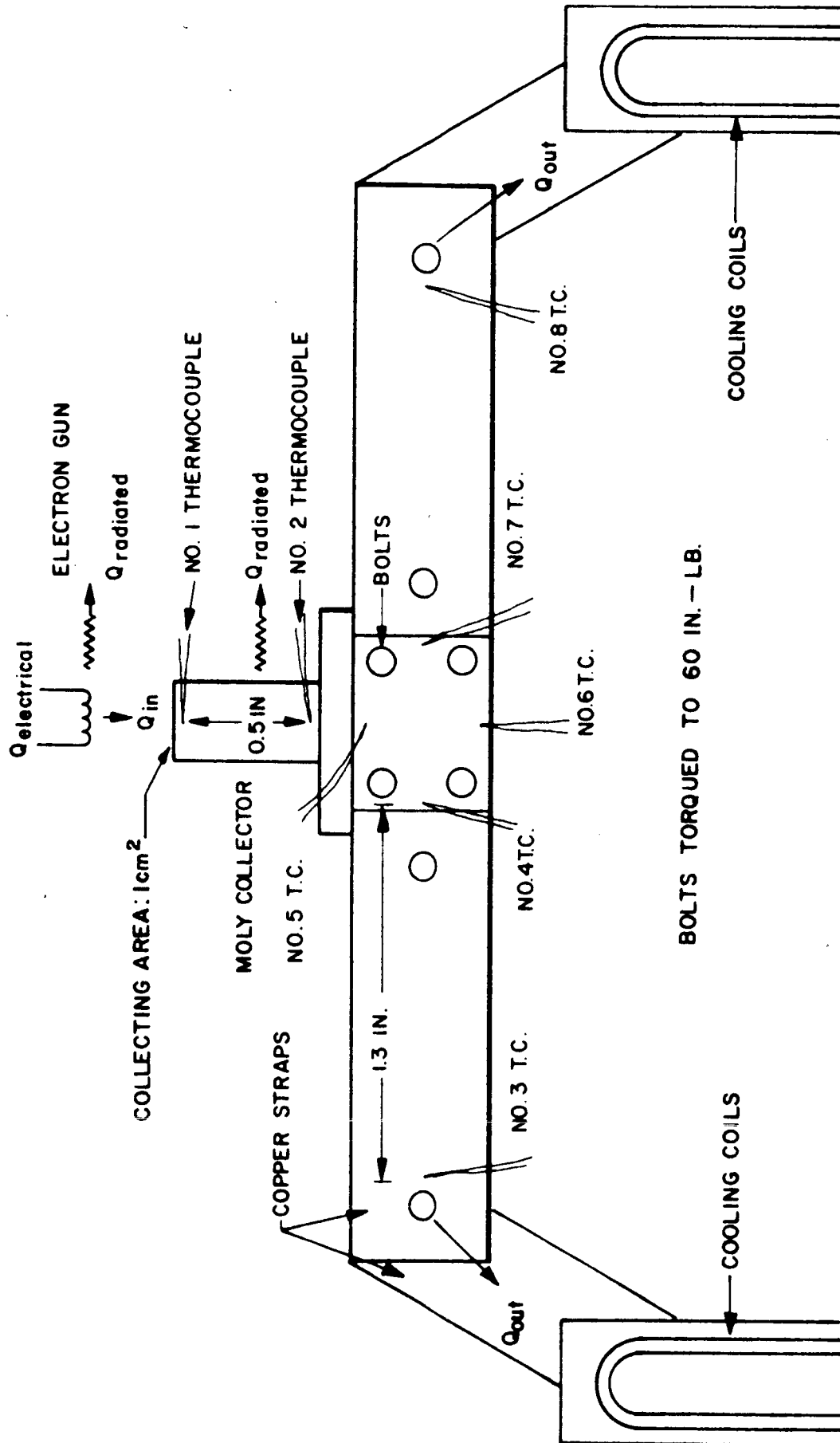


FIG. 2-2 SETUP FOR COLLECTOR HEAT TRANSFER EXPERIMENT

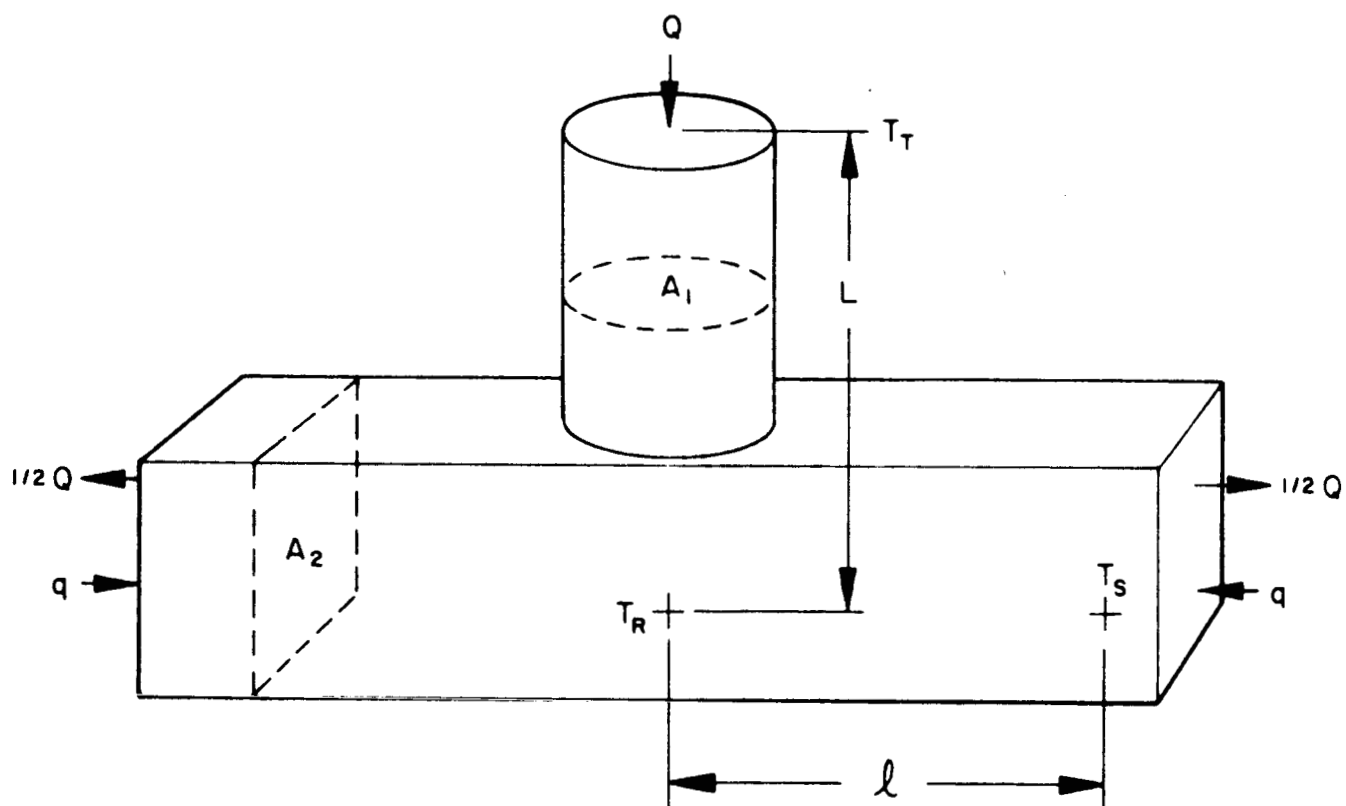


FIG. 2-3 IDEALIZED COLLECTOR-RADIATOR SYSTEM

power into each radiator strap,  $T_T$  is the collector top temperature,  $T_r$  is the collector root temperature, and  $T_s$  is the collector radiator strap temperature. Now,

$$Q = \frac{k_1 A_1 (T_T - T_r)}{L} \quad (8)$$

and

$$1/2Q - q = \frac{k_2 A_2 (T_r - T_s)}{1}, \quad (9)$$

where  $k_1$ ,  $k_2$ ,  $A_1$ , and  $A_2$  are the conductivities and cross-sectional areas of the collector and radiator strap, respectively. Combining Eqs. 8 and 9 and solving for  $T_r$  yields:

$$T_r = \frac{\left(\frac{k_1 A_1}{L}\right) T_T + \left(\frac{2k_2 A_2}{1}\right) T_s - 2q}{\frac{k_1 A_1}{L} + \frac{2k_2 A_2}{1}} \quad (10)$$

Equation 10 is used to determine the heater power necessary to control the collector temperatures. If a collector surface temperature of  $700^\circ\text{C}$  is desired, the required heater power can be calculated. In addition to  $T_T = 700^\circ\text{C}$ , it will be assumed that  $T_r = 500^\circ\text{C}$  and  $T_s = 450^\circ\text{C}$ . Thus, Eq. 10 yields  $q = 70$  watts for the geometry of the designed collector radiator.

Figure 2-4 shows the variation of collector face temperature with collector current density. The curve was calculated assuming a constant collector root temperature of  $450^\circ\text{C}$ . The significance of Fig. 2-4 lies in the result that steady-state optimized power measurements will be limited to currents less than  $125 \text{ amperes/cm}^2$ . This is due to EOS' experience that minimum collector work functions cannot be achieved for collector temperatures in excess of  $900^\circ\text{C}$ . This result does not place a limitation on emission measurements at much higher current densities than  $125 \text{ amperes/cm}^2$ . When optimized power output is of no interest, the allowable collector surface temperature

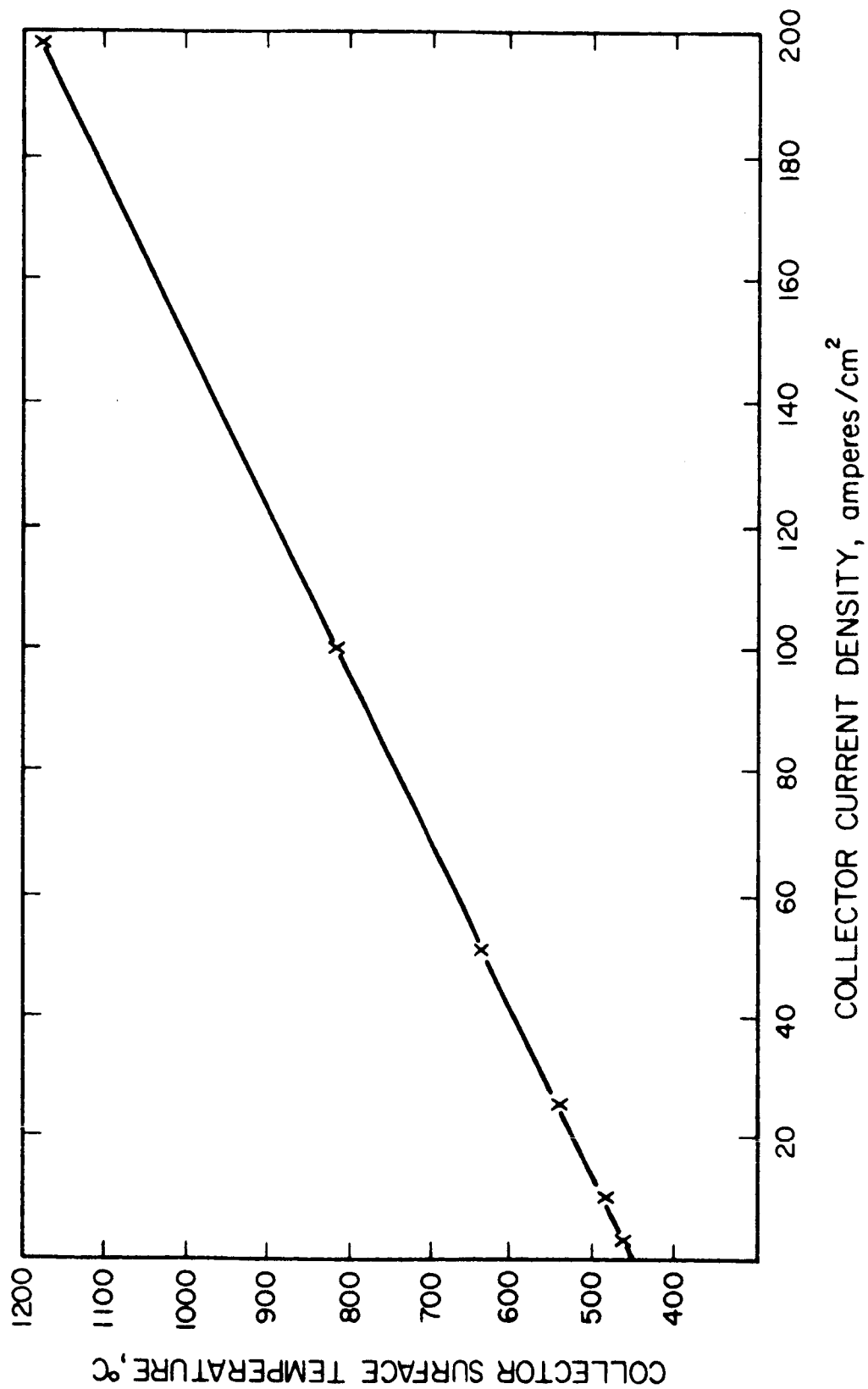


FIG. 2-4 COLLECTOR SURFACE TEMPERATURE AS A FUNCTION OF COLLECTOR CURRENT DENSITY (Calculated)

is limited only by structural considerations; therefore, currents of 200 amperes/cm<sup>2</sup> can be easily measured.

Figures 2-5 and 2-6 are plots of the approximate distribution of isotherms down the lengths of the members. The distributions were obtained using a teledeltos analog electrical field plotter. The cross section through the collector barrel is in a plane perpendicular to the radiator heat sink strap. These plots are to indicate that a uniform heat transfer will take place at the collector radiator interface resulting from a uniform temperature at the collector root.

#### 2.1.1.2 Interelectrode Potential Distribution and Analysis

Utilizing the teledeltos analog field plotter, an interelectrode electrostatic potential distribution was obtained for an equivalent interelectrode spacing of 5 mils for three cases: (1) the guard ring at the same potential as the collector; (2) the guard ring at a potential intermediate between those of the collector and emitter; and (3) the collector at a potential between those of the guard ring and emitter. For the first case, the penetration potential in the collector-guard ring gap is reduced to 1 percent of the collector-emitter potential in one gap width. This situation is shown in Fig. 2-7. In addition, the shifts in the potential distribution as the guard ring potential varies are evident.

There are two major conclusions to be drawn from these distributions: (1) the potential distribution in the interelectrode area between emitter and collector is insensitive to guard ring potential; and (2) the maximum error in the emission area determination is less than 2 percent. These conclusions result from observing that with deviations of the guard ring potential as large as  $\pm 10$  percent, the potential distribution perturbations within the interelectrode space due to guard ring potential variations are completely suppressed in a distance only 0.002 inch from the edge of the collector

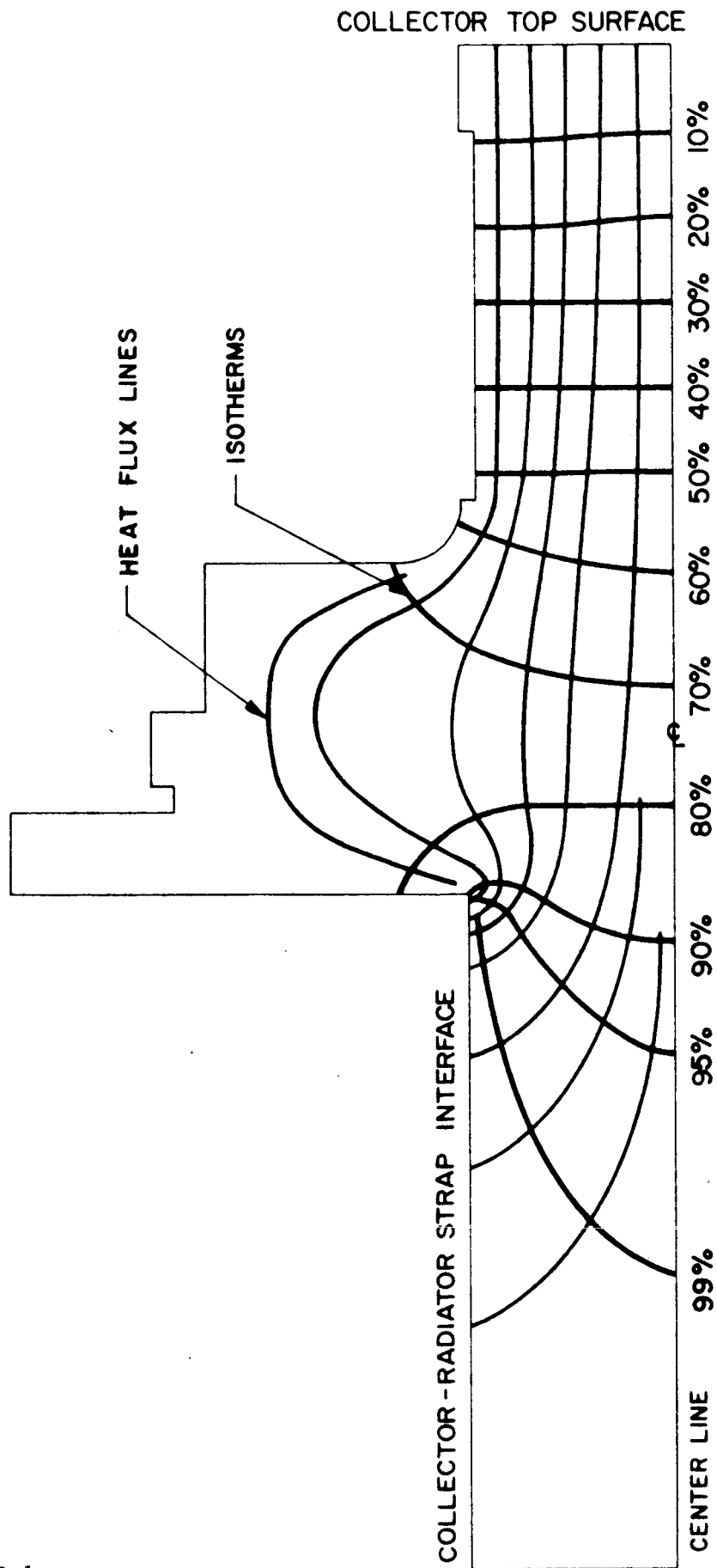


FIG. 2-5 COLLECTOR ISOTHERM DISTRIBUTION

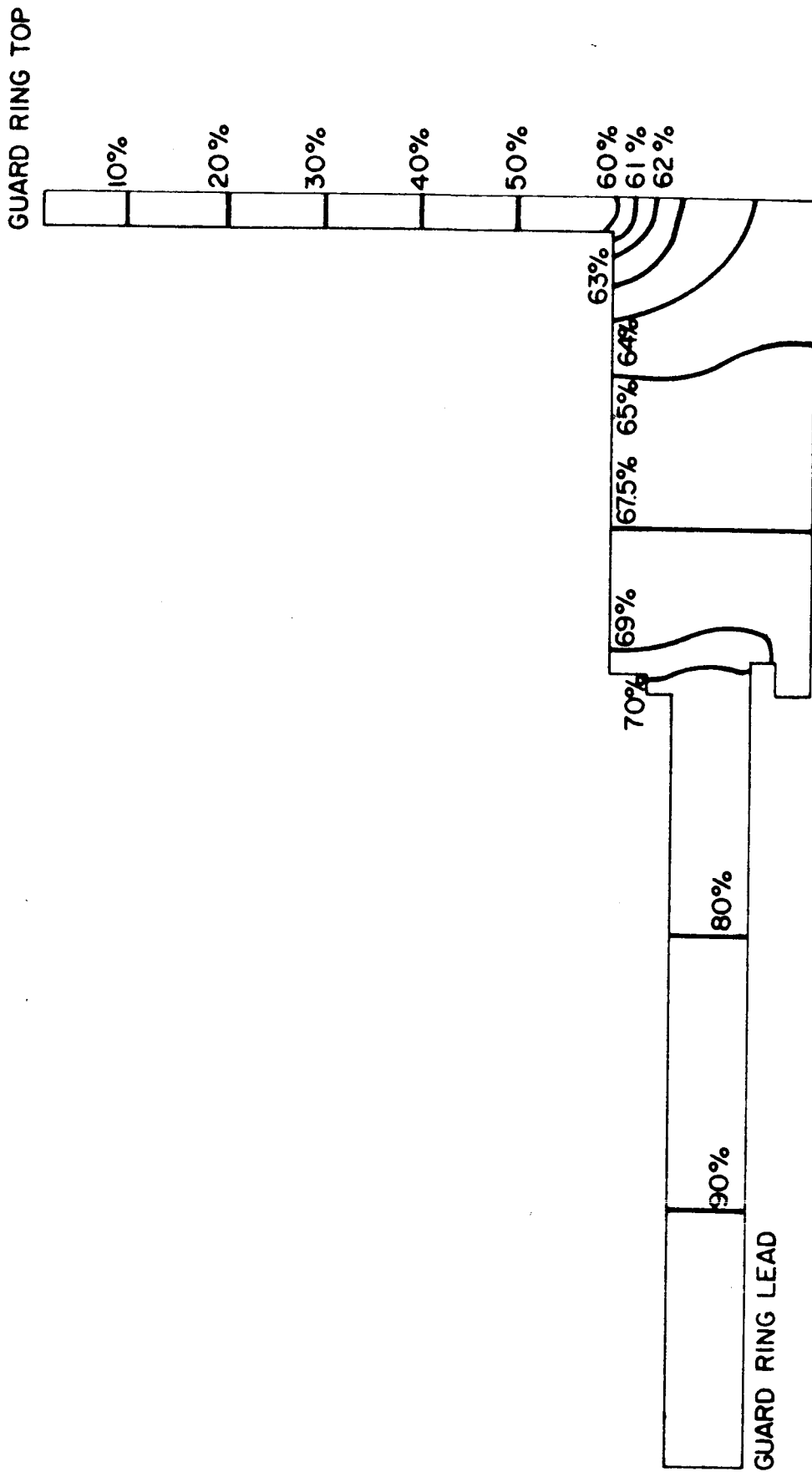
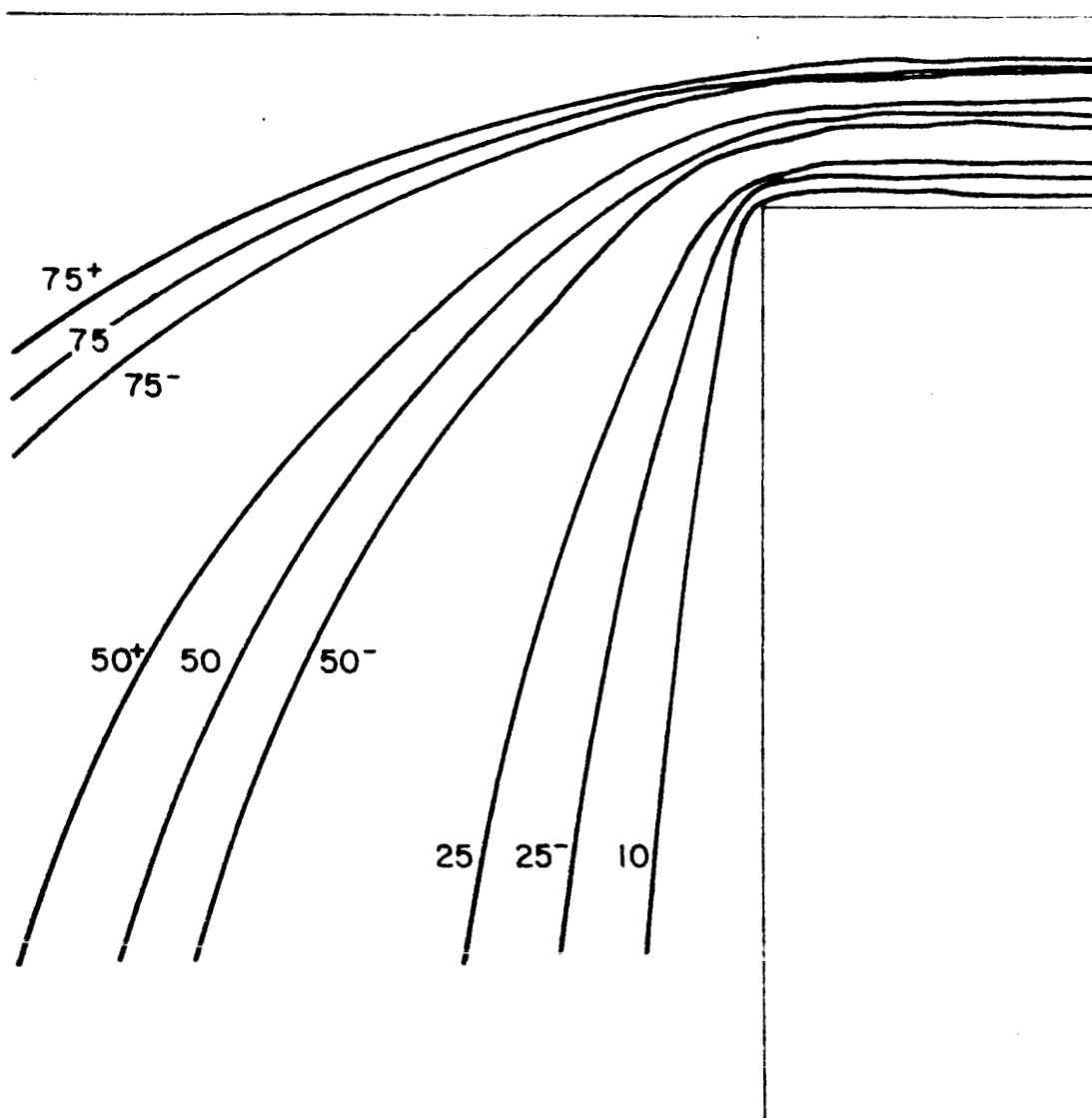


FIG. 2-6 GUARD RING ISOTHERM DISTRIBUTION



## EMITTER STRUCTURE

## GUARD RING STRUCTURE

### LEGEND:

- + DENOTES GUARD RING AT HIGHER (10%)  
POTENTIAL THAN COLLECTOR
- DENOTES GUARD RING AT LOWER (10%)  
POTENTIAL THAN COLLECTOR  
(RING POTENTIAL BETWEEN EMITTER  
& CELL)
- NO SIGN DENOTES GUARD RING AND  
COLLECTOR ARE AT SAME POTENTIAL

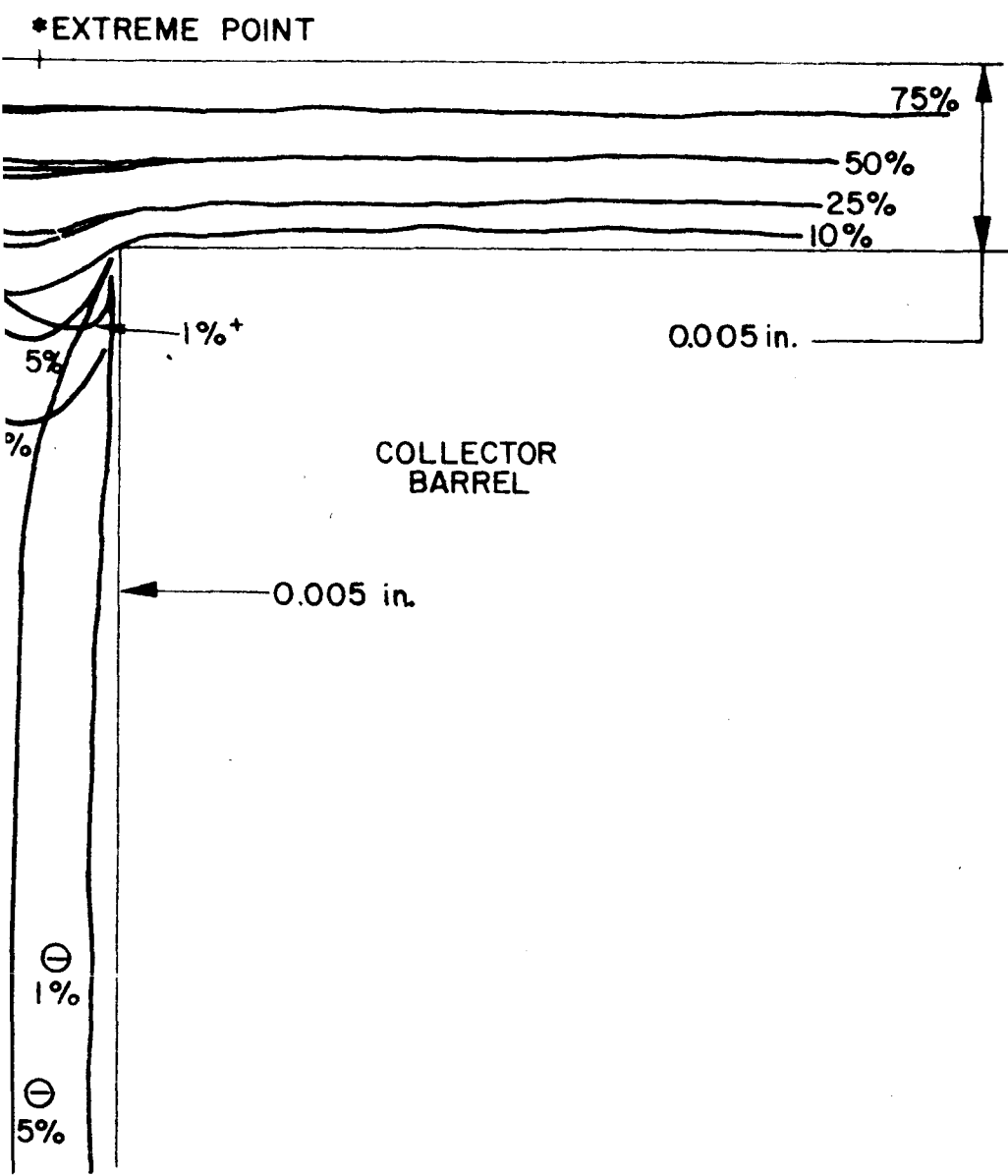


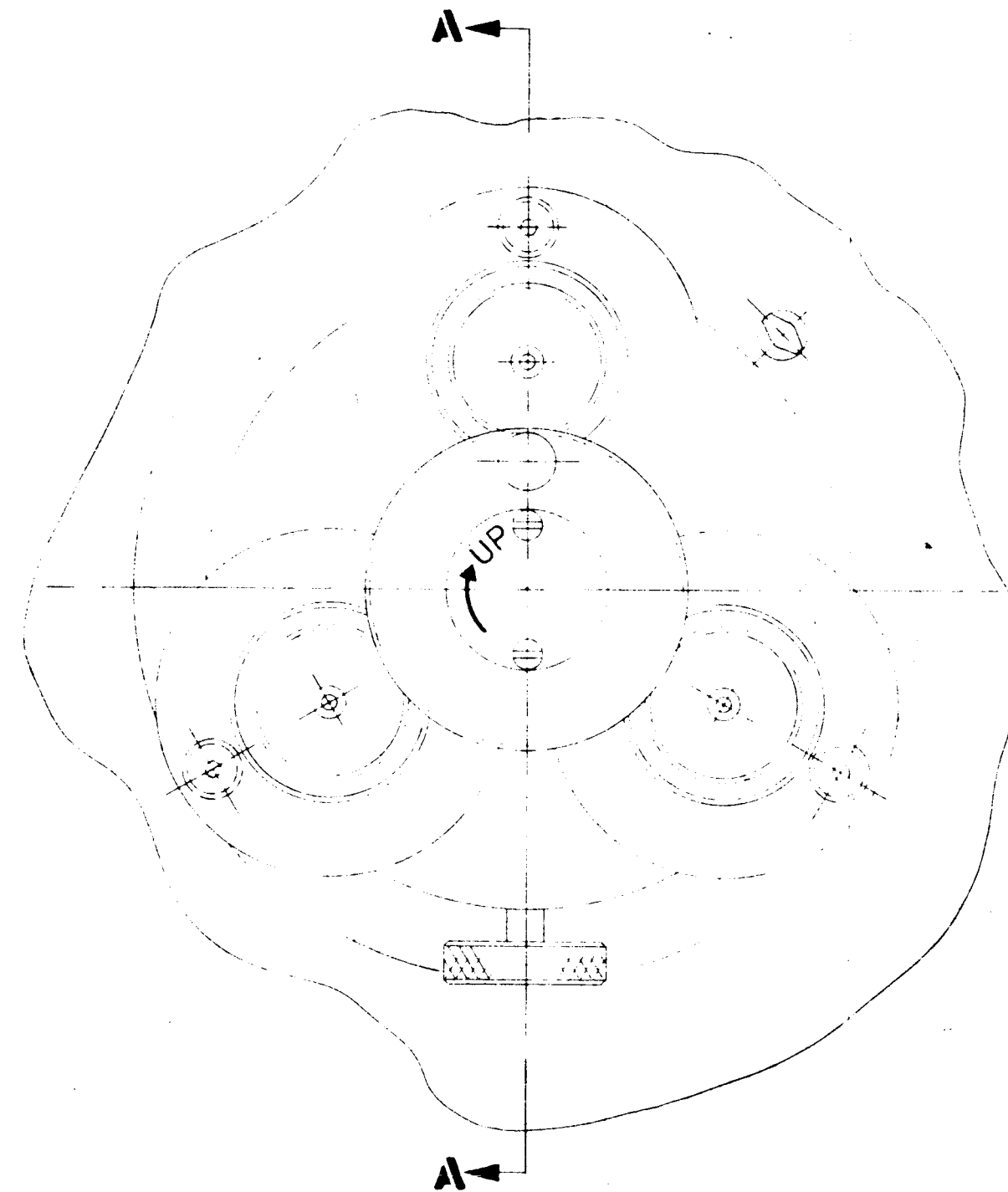
FIG. 2-7 INTERELECTRODE POTENTIAL DISTRIBUTIONS

surface. The estimate of emission area error is based on the symmetry of the potential lines. The line of electrostatic potential symmetry bisects the guard ring-collector gap. The drift electrons in the interelectrode spacing have thermal energies of only approximately 0.5 volts. If the energies of the drift electrons are comparable to or less than the potential drop of the spacing, the electron trajectories are essentially perpendicular to the potential lines. If the electron energies are much greater than the total potential drop in the gap, they are free to travel at large angles to the potential lines. In the case of a thermionic converter, approximately the total potential drop is across the sheath at the cathode, since the interelectrode spacing is predominately a very weak field region. In this case, though, the drift electrons enter the emitter sheath from the emitter (cathode) with energies of only  $2kT$  and, with the very steep potential gradient in the sheath, they are easily forced into a trajectory of normal incidence. Therefore, it seems apparent that the farthest point from the collector (anode) from which electrons can originate and be collected by the collector is the point on the emitter opposite the midpoint of the collector-guard ring spacing. This point has been marked in Fig. 2-7. Using this point for measuring the emitting area results in a maximum effective emitter area of  $2.04 \text{ cm}^2$ , an error of 2 percent in the desired emitter area of  $2.00 \text{ cm}^2$ .

These potential plots were made for the vacuum case. In a plasma-filled environment with a cathode sheath, the sheath acts as a virtual cathode and the potential distribution in the plasma column is still represented by the indicated teledeltos plots.

#### 2.1.1.3 Drive Mechanism

The emitter-collector spacing on the variable parameter test vehicle is varied by applying force to three spring-loaded rods which are inserted from the bell jar top plate. These rods apply pressure to the emitter plate seen in Fig. 2-8. The individual rods are

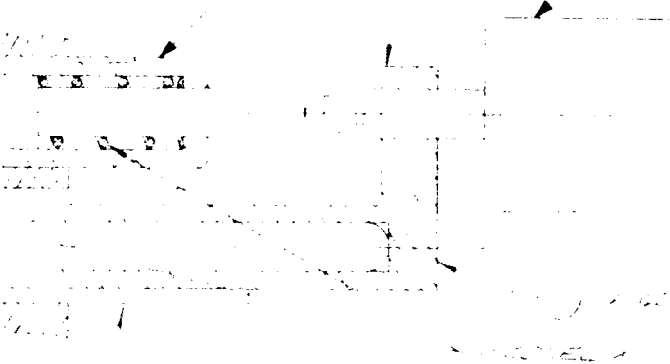






STAINLESS  
STEEL TYPE 304

MEASURING DEVICE



1	1/2" DIA. FLANGE	3	6
1	1/2" DIA. FLANGE	3	15
1	STAINLESS	3	4
1	OUTER HOUSING	3	13
1	INNER HOUSING	3	12
1	1/2" DIA. FLANGE	3	11
1	1/2" DIA. FLANGE	3	10
1	HOUSING HOUSING	3	9
1	HOUSING HOUSING	3	8
1	HOUSING HOUSING	3	7
1	HOUSING HOUSING	3	6
1	HOUSING HOUSING	3	5
1	HOUSING HOUSING	3	4
1	HOUSING HOUSING	3	3
1	HOUSING HOUSING	3	2
1	HOUSING HOUSING	3	1

DASH NO.	DESCRIPTION	SPECIFICATION	STANDARD	MATERIAL	NO. REQD.	ZONE	P.N.O.

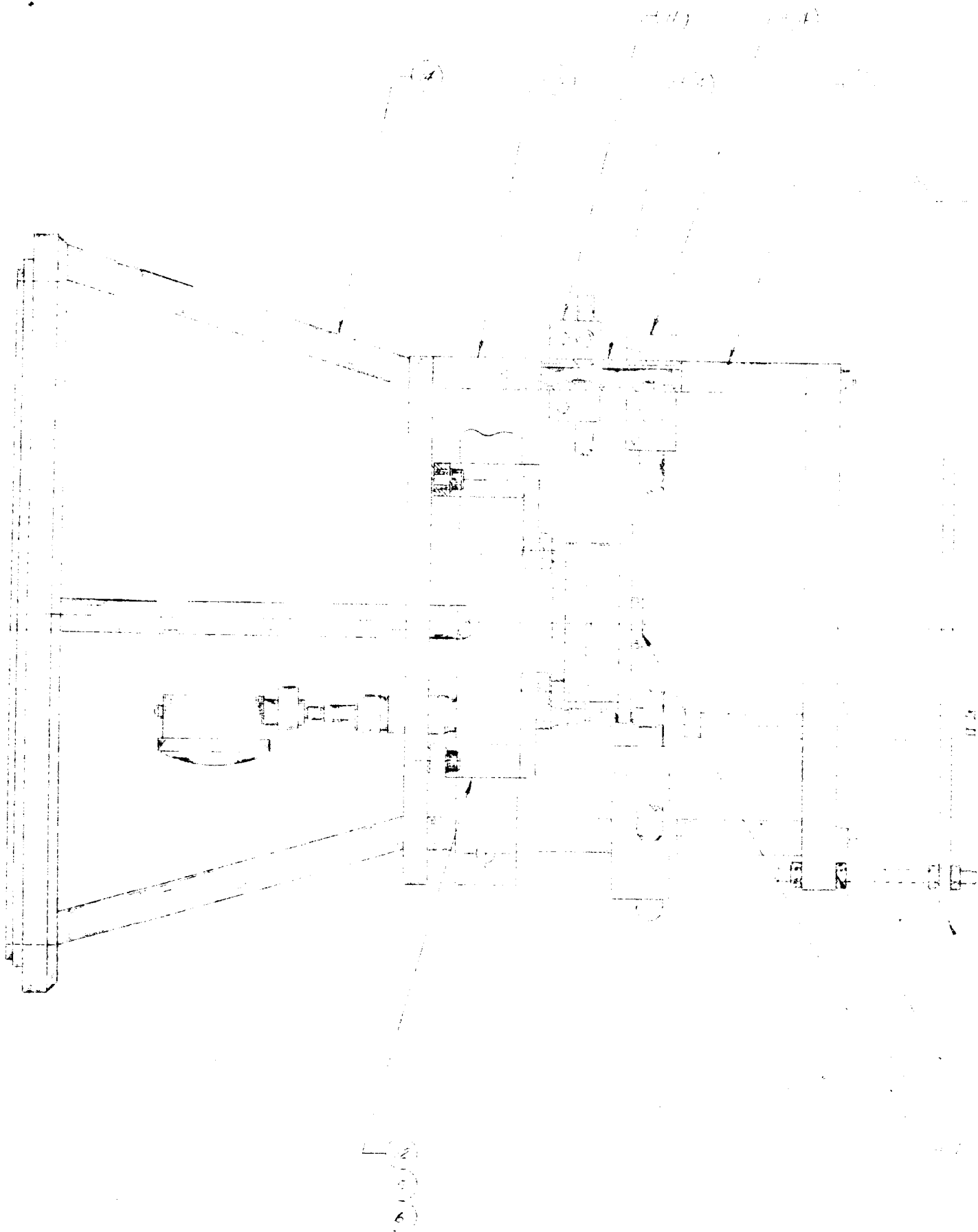
JET PROPULSION LABORATORY CALIFORNIA INSTITUTE OF TECHNOLOGY BUILDING 180-100 SECT. 100-100	J 140500 SHEET 2 OF 7 REVISION
--	--------------------------------------

controlled by a differential thread drive to allow independent movement of each rod. One complete rotation of the control nut on the individual rods results in a translational movement of 0.002 inch. The three rods can be ganged for uniform motion controlled with a single drive. One complete rotation of the main control knob results in a uniform movement of 0.0008 inch by the ganged rods. The return movement is obtained by spring-loaded ceramic rods mounted beneath the emitter plate. These rods keep a constant expanding pressure on the bellows section of the vehicle. The spacing measurement device is also mounted beneath the emitter plate. The measuring device is supported from a second ceramic rod while measuring the movement of the ceramic return rod. This temperature compensating method allows the measuring device to indicate only true mechanical movement of the emitter with respect to the collector and not the thermal expansion in the support and return rods. The measuring device will be a dial-gauge depth indicator accurate to 0.0001 inch. The ganged drive housing has been machined, in addition to the three sets of differential thread drives. Orders have been placed for all required material and components.

#### 2.1.1.4 Support Fixtures

All of the preceding thermal considerations are irrelevant if there are no adequate means for carrying the electrical currents and thermal loads into and away from the emission test vehicle. In addition, the precision mechanical support of the vehicle is of major importance.

Figure 2-9 shows the approach taken. The basic support structure consists of three stainless steel disks separated by stainless steel rods. The bottom disk mates with the inside diameter of the vacuum test station base plate. The middle disk supports the return drive mechanism and the actual vehicle support straps. This disk is covered by ten sheets of 0.002-inch-thick dimpled molybdenum heat shields. The shields are necessary to limit the maximum temperature of the dial indicator suspended below this stainless steel



This technical drawing shows a cross-section of a mechanical component, possibly a pump or engine part. It features a cylindrical main body with a flange at the bottom. The interior of the cylinder contains several internal components, including what appears to be a central shaft or piston rod. The drawing is a black and white line drawing, typical of engineering schematics.

40565	-1	SUB ASSY W/DR DATE 10-22-69
40563	-1	ELUB
40562	-1	SEALLET
40561	-1	SUB ASSY W/DR DATE 10-22-69
40553	-1	INSULATOR
40552	-1	ROL
40551	-1	STAND OFF
40550	-1	SUPPORT
40548	-2	INSULATOR
40548	-1	INSULATOR
40522	-1	GRASSY EXTERIOR PLUG
40520	-1	REPAIRING PLUG W/INSTR FOR USE
40519	-1	W/INSTR FOR USE
40518	-1	W/INSTR FOR USE
40517	-1	W/INSTR FOR USE
40516	-1	W/INSTR FOR USE
40515	-1	W/INSTR FOR USE
40514	-1	W/INSTR FOR USE
40513	-1	W/INSTR FOR USE
40512	-1	W/INSTR FOR USE
40511	-1	W/INSTR FOR USE
40510	-1	W/INSTR FOR USE
40509	-1	W/INSTR FOR USE
40508	-1	W/INSTR FOR USE
40507	-1	W/INSTR FOR USE
40506	-1	W/INSTR FOR USE
40505	-1	W/INSTR FOR USE
40504	-1	W/INSTR FOR USE
40503	-1	W/INSTR FOR USE
40502	-1	W/INSTR FOR USE
40501	-1	W/INSTR FOR USE
40500	-1	W/INSTR FOR USE
40499	-1	W/INSTR FOR USE
40498	-1	W/INSTR FOR USE
40497	-1	W/INSTR FOR USE
40496	-1	W/INSTR FOR USE
40495	-1	W/INSTR FOR USE
40494	-1	W/INSTR FOR USE
40493	-1	W/INSTR FOR USE
40492	-1	W/INSTR FOR USE
40491	-1	W/INSTR FOR USE
40490	-1	W/INSTR FOR USE
40489	-1	W/INSTR FOR USE
40488	-1	W/INSTR FOR USE
40487	-1	W/INSTR FOR USE
40486	-1	W/INSTR FOR USE
40485	-1	W/INSTR FOR USE
40484	-1	W/INSTR FOR USE
40483	-1	W/INSTR FOR USE
40482	-1	W/INSTR FOR USE
40481	-1	W/INSTR FOR USE
40480	-1	W/INSTR FOR USE
40479	-1	W/INSTR FOR USE
40478	-1	W/INSTR FOR USE
40477	-1	W/INSTR FOR USE
40476	-1	W/INSTR FOR USE
40475	-1	W/INSTR FOR USE
40474	-1	W/INSTR FOR USE
40473	-1	W/INSTR FOR USE
40472	-1	W/INSTR FOR USE
40471	-1	W/INSTR FOR USE
40470	-1	W/INSTR FOR USE
40469	-1	W/INSTR FOR USE
40468	-1	W/INSTR FOR USE
40467	-1	W/INSTR FOR USE
40466	-1	W/INSTR FOR USE
40465	-1	W/INSTR FOR USE
40464	-1	W/INSTR FOR USE
40463	-1	W/INSTR FOR USE
40462	-1	W/INSTR FOR USE
40461	-1	W/INSTR FOR USE
40460	-1	W/INSTR FOR USE
40459	-1	W/INSTR FOR USE
40458	-1	W/INSTR FOR USE
40457	-1	W/INSTR FOR USE
40456	-1	W/INSTR FOR USE
40455	-1	W/INSTR FOR USE
40454	-1	W/INSTR FOR USE
40453	-1	W/INSTR FOR USE
40452	-1	W/INSTR FOR USE
40451	-1	W/INSTR FOR USE
40450	-1	W/INSTR FOR USE
40449	-1	W/INSTR FOR USE
40448	-1	W/INSTR FOR USE
40447	-1	W/INSTR FOR USE
40446	-1	W/INSTR FOR USE
40445	-1	W/INSTR FOR USE
40444	-1	W/INSTR FOR USE
40443	-1	W/INSTR FOR USE
40442	-1	W/INSTR FOR USE
40441	-1	W/INSTR FOR USE
40440	-1	W/INSTR FOR USE
40439	-1	W/INSTR FOR USE
40438	-1	W/INSTR FOR USE
40437	-1	W/INSTR FOR USE
40436	-1	W/INSTR FOR USE
40435	-1	W/INSTR FOR USE
40434	-1	W/INSTR FOR USE
40433	-1	W/INSTR FOR USE
40432	-1	W/INSTR FOR USE
40431	-1	W/INSTR FOR USE
40430	-1	W/INSTR FOR USE
40429	-1	W/INSTR FOR USE
40428	-1	W/INSTR FOR USE
40427	-1	W/INSTR FOR USE
40426	-1	W/INSTR FOR USE
40425	-1	W/INSTR FOR USE
40424	-1	W/INSTR FOR USE
40423	-1	W/INSTR FOR USE
40422	-1	W/INSTR FOR USE
40421	-1	W/INSTR FOR USE
40420	-1	W/INSTR FOR USE
40419	-1	W/INSTR FOR USE
40418	-1	W/INSTR FOR USE
40417	-1	W/INSTR FOR USE
40416	-1	W/INSTR FOR USE
40415	-1	W/INSTR FOR USE
40414	-1	W/INSTR FOR USE
40413	-1	W/INSTR FOR USE
40412	-1	W/INSTR FOR USE
40411	-1	W/INSTR FOR USE
40410	-1	W/INSTR FOR USE
40409	-1	W/INSTR FOR USE
40408	-1	W/INSTR FOR USE
40407	-1	W/INSTR FOR USE
40406	-1	W/INSTR FOR USE
40405	-1	W/INSTR FOR USE
40404	-1	W/INSTR FOR USE
40403	-1	W/INSTR FOR USE
40402	-1	W/INSTR FOR USE
40401	-1	W/INSTR FOR USE
40400	-1	W/INSTR FOR USE
40399	-1	W/INSTR FOR USE
40398	-1	W/INSTR FOR USE
40397	-1	W/INSTR FOR USE
40396	-1	W/INSTR FOR USE
40395	-1	W/INSTR FOR USE
40394	-1	W/INSTR FOR USE
40393	-1	W/INSTR FOR USE
40392	-1	W/INSTR FOR USE
40391	-1	W/INSTR FOR USE
40390	-1	W/INSTR FOR USE
40389	-1	W/INSTR FOR USE
40388	-1	W/INSTR FOR USE
40387	-1	W/INSTR FOR USE
40386	-1	W/INSTR FOR USE
40385	-1	W/INSTR FOR USE
40384	-1	W/INSTR FOR USE
40383	-1	W/INSTR FOR USE
40382	-1	W/INSTR FOR USE
40381	-1	W/INSTR FOR USE
40380	-1	W/INSTR FOR USE
40379	-1	W/INSTR FOR USE
40378	-1	W/INSTR FOR USE
40377	-1	W/INSTR FOR USE
40376	-1	W/INSTR FOR USE
40375	-1	W/INSTR FOR USE
40374	-1	W/INSTR FOR USE
40373	-1	W/INSTR FOR USE
40372	-1	W/INSTR FOR USE
40371	-1	W/INSTR FOR USE
40370	-1	W/INSTR FOR USE
40369	-1	W/INSTR FOR USE
40368	-1	W/INSTR FOR USE
40367	-1	W/INSTR FOR USE
40366	-1	W/INSTR FOR USE
40365	-1	W/INSTR FOR USE
40364	-1	W/INSTR FOR USE
40363	-1	W/INSTR FOR USE
40362	-1	W/INSTR FOR USE
40361	-1	W/INSTR FOR USE
40360	-1	W/INSTR FOR USE
40359	-1	W/INSTR FOR USE
40358	-1	W/INSTR FOR USE
40357	-1	W/INSTR FOR USE
40356	-1	W/INSTR FOR USE
40355	-1	W/INSTR FOR USE
40354	-1	W/INSTR FOR USE
40353	-1	W/INSTR FOR USE
40352	-1	W/INSTR FOR USE
40351	-1	W/INSTR FOR USE
40350	-1	W/INSTR FOR USE
40349	-1	W/INSTR FOR USE
40348	-1	W/INSTR FOR USE
40347	-1	W/INSTR FOR USE
40346	-1	W/INSTR FOR USE
40345	-1	W/INSTR FOR USE
40344	-1	W/INSTR FOR USE
40343	-1	W/INSTR FOR USE
40342	-1	W/INSTR FOR USE
40341	-1	W/INSTR FOR USE
40340	-1	W/INSTR FOR USE
40339	-1	W/INSTR FOR USE
40338	-1	W/INSTR FOR USE
40337	-1	W/INSTR FOR USE
40336	-1	W/INSTR FOR USE
40335	-1	W/INSTR FOR USE
40334	-1	W/INSTR FOR USE
40333	-1	W/INSTR FOR USE
40332	-1	W/INSTR FOR USE
40331	-1	W/INSTR FOR USE
40330	-1	W/INSTR FOR USE
40329	-1	W/INSTR FOR USE
40328	-1	W/INSTR FOR USE
40327	-1	W/INSTR FOR USE
40326	-1	W/INSTR FOR USE
40325	-1	W/INSTR FOR USE
40324	-1	W/INSTR FOR USE
40323	-1	W/INSTR FOR USE
40322	-1	W/INSTR FOR USE
40321	-1	W/INSTR FOR USE
40320	-1	W/INSTR FOR USE
40319	-1	W/INSTR FOR USE
40318	-1	W/INSTR FOR USE
40317	-1	W/INSTR FOR USE
40316	-1	W/INSTR FOR USE
40315	-1	W/INSTR FOR USE
40314	-1	W/INSTR FOR USE
40313	-1	W/INSTR FOR USE
40312	-1	W/INSTR FOR USE
40311	-1	W/INSTR FOR USE
40310	-1	W/INSTR FOR USE
40309	-1	W/INSTR FOR USE
40308	-1	W/INSTR FOR USE
40307	-1	W/INSTR FOR USE
40306	-1	W/INSTR FOR USE
40305	-1	W/INSTR FOR USE
40304	-1	W/INSTR FOR USE
40303	-1	W/INSTR FOR USE
40302	-1	W/INSTR FOR USE
40301	-1	W/INSTR FOR USE
40300	-1	W/INSTR FOR USE
40299	-1	W/INSTR FOR USE
40298	-1	W/INSTR FOR USE
40297	-1	W/INSTR FOR USE
40296	-1	W/INSTR FOR USE
40295	-1	W/INSTR FOR USE
40294	-1	W/INSTR FOR USE
40293	-1	W/INSTR FOR USE
40292	-1	W/INSTR FOR USE
40291	-1	W/INSTR FOR USE
40290	-1	W/INSTR FOR USE
40289	-1	W/INSTR FOR USE
40288	-1	W/INSTR FOR USE
40287	-1	W/INSTR FOR USE
40286	-1	W/INSTR FOR USE
40285	-1	W/INSTR FOR USE
40284	-1	W/INSTR FOR USE
40283	-1	W/INSTR FOR USE
40282	-1	W/INSTR FOR USE
40281	-1	W/INSTR FOR USE
40280	-1	W/INSTR FOR USE
40279	-1	W/INSTR FOR USE
40278	-1	W/INSTR FOR USE
40277	-1	W/INSTR FOR USE
40276	-1	W/INSTR FOR USE
40275	-1	W/INSTR FOR USE
40274	-1	W/INSTR FOR USE
40273	-1	W/INSTR FOR USE
40272	-1	W/INSTR FOR USE
40271	-1	W/INSTR FOR USE
40270	-1	W/INSTR FOR USE
40269	-1	W/INSTR FOR USE
40268	-1	W/INSTR FOR USE
40267	-1	W/INSTR FOR USE
40266	-1	W/INSTR FOR USE
40265	-1	W/INSTR FOR USE
40264	-1	W/INSTR FOR USE
40263	-1	W/INSTR FOR USE
40262	-1	W/INSTR FOR USE
40261	-1	W/INSTR FOR USE
40260	-1	W/INSTR FOR USE
40259	-1	W/INSTR FOR USE
40258	-1	W/INSTR FOR USE
40257	-1	W/INSTR FOR USE
40256	-1	W/INSTR FOR USE
40255	-1	W/INSTR FOR USE
40254	-1	W/INSTR FOR USE
40253	-1	W/INSTR FOR USE
40252	-1	W/INSTR FOR USE
40251	-1	W/INSTR FOR USE
40250	-1	W/INSTR FOR USE
40249	-1	W/INSTR FOR USE
40248	-1	W/INSTR FOR USE
40247	-1	W/INSTR FOR USE
40246	-1	W/INSTR FOR USE
40245	-1	W/INSTR FOR USE
40244	-1	W/INSTR FOR USE
40243	-1	W/INSTR FOR USE
40242	-1	W/INSTR FOR USE
40241	-1	W/INSTR FOR USE
40240	-1	W/INSTR FOR USE
40239	-1	W/INSTR FOR USE
40238	-1	W/INSTR FOR USE
40237	-1	W/INSTR FOR USE
40236	-1	W/INSTR FOR USE
40235	-1	W/INSTR FOR USE
40234	-1	W/INSTR FOR USE
40233	-1	W/INSTR FOR USE
40232	-1	W/INSTR FOR USE
40231	-1	W/INSTR FOR USE
40230	-1	W/INSTR FOR USE
40229	-1	W/INSTR FOR USE
40228	-1	W/INSTR FOR USE
40227	-1	W/INSTR FOR USE
40226	-1	W/INSTR FOR USE
40225	-1	W/INSTR FOR USE
40224	-1	W/INSTR FOR USE
40223	-1	W/INSTR FOR USE
40222	-1	W/INSTR FOR USE
40221	-1	W/INSTR FOR USE
40220	-1	W/INSTR FOR USE
40219	-1	W/INSTR FOR USE
40218	-1	W/INSTR FOR USE
40217	-1	W/INSTR FOR USE
40216	-1	W/INSTR FOR USE
40215	-1	W/INSTR FOR USE
40214	-1	W/INSTR FOR USE
40213	-1	W/INSTR FOR USE
40212	-1	W/INSTR FOR USE
40211	-1	W/INSTR FOR USE
40210	-1	W/INSTR FOR USE
40209	-1	W/INSTR FOR USE
40208	-1	W/INSTR FOR USE
40207	-1	W/INSTR FOR USE
40206	-1	W/INSTR FOR USE
40205	-1	W/INSTR FOR USE
40204	-1	W/INSTR FOR USE
40203	-1	W/INSTR FOR USE
40202	-1	W/INSTR FOR USE
40201	-1	W/INSTR FOR USE
40200	-1	W/INSTR FOR USE
40199	-1	W/INSTR FOR USE
40198	-1	W/INSTR FOR USE
40197	-1	

# 0. ENGINE STRUCTURE LAYOUT

			1	4
			1	13
			2	12
			1	11
			3	10
			3	9
			3	8
			1	7
			4	6
			2	5
			1	4
				3
			1	2
			1	1
SPE. LOCATION	NO. REQD.	2. NO.	3. NO.	4. NO.
VARIABLE SPACING EMISSION TEST VEHICLE		JET PROPULSION LABORATORY CALIFORNIA INSTITUTE OF TECHNOLOGY		
DESIGNED BY		RELEASED THROUGH SECT.		
CHECKED BY		J 140527		
APPROVED BY		SHEET 1 OF 1		
CLASSIFICATION		REVISION		
SCALE				

disk. Two molybdenum straps are connected to the collector root and terminate on the stainless steel disk, as shown in the figure, to provide mechanical support. The electron bombardment gun is suspended from the upper disk. As the interelectrode spacing is varied, the gun remains stationary. Since the interelectrode spacing variation will only be approximately 0.010 inch it is felt that the emitter temperature variation caused by this corresponding gun-to-emitter spacing variation can be controlled with a fine adjust potentiometer on the bombardment voltage. This scheme has proven to be successful in past EOS experiments on variable spacing vehicles.

The electrical connections are made in the following manner. The collector radiator straps are connected by flexible straps to copper bus bars equipped with copper cooling coils on both sides of the device. The guard ring and emitter connections are made with closed copper tubes which double as water-cooling coils and current conductors. Since the emitter carries a much higher current load than the guard ring, the cross-sectional area of the emitter tubing wall is greater than that of the guard ring copper conductor in order to limit the current density to less than 500 amperes/cm<sup>2</sup>. If the water is taken into account, the current density in the leads is reduced drastically. The two copper rings are supported at the stainless steel supports and insulated by a ceramic sleeve. Thin copper straps make the connection between the emitter and guard ring and their respective rings at three positions symmetrically positioned around the ring.

As the straps heat up from the electrical current, their thermal expansion creates a stress force on the guard ring and emitter lead flanges. Due to smaller size of the guard ring flanges, this force must be given consideration. The stress force can be calculated from classical considerations:

$$F = AY \frac{\Delta L}{L} ,$$

where  $A$  is the cross-sectional area,  $Y$  is Young's modulus of copper, and  $\frac{\Delta L}{L}$  is the percentage expansion of the strap. A conservative calculation is to use Young's modulus at room temperature, since  $Y$  decreases with increasing temperature. If 0.010-inch-thick straps 0.500 inch wide are used and a temperature drop of  $300^{\circ}\text{C}$  is assumed, the resulting stress force is calculated to be 0.4 pound from each strap to the guard ring lead. Now, if a vee section is put in the strap, vector resolution of the resulting forces indicates that the vertical components cancel each other and the horizontal components of the stress force are reduced by the sine of the angle of the vee. If a 20-degree angle is assumed and with the same parameters as used previously, the force is reduced to 0.036 pound at the guard ring. Therefore, it can be concluded that the guard ring positioning will not be affected by stress forces resulting from thermal loads through the lead straps.

#### 2.1.2 Vehicle Fabrication

The variable parameter test vehicle design shown in Fig. 2-10 has a concentric geometry; the emitter envelope, guard ring, and collector barrel are concentric about a common axis. This design permits the accurate micro-optical pyrometer measurement of emitter temperatures by means of an 8-to-1 black-body hole without obstruction by the bombardment filament. This geometry also minimizes the possible establishment of a parasitic cesium vapor reservoir due to the operation of some structural members of the vehicle at temperatures near, or lower than, the cesium reservoir proper.

The emitter may be replaced by cutting the heli-arc weld of the copper bellows seal and removing the emitter plate and envelope. Replacement of the collector is accomplished in the same fashion. The replacement of the collector permits the study of different collector surface materials. The guard ring should be made of the same material as the collector so that identical cesiated surface work functions and zero contact potential can be maintained between

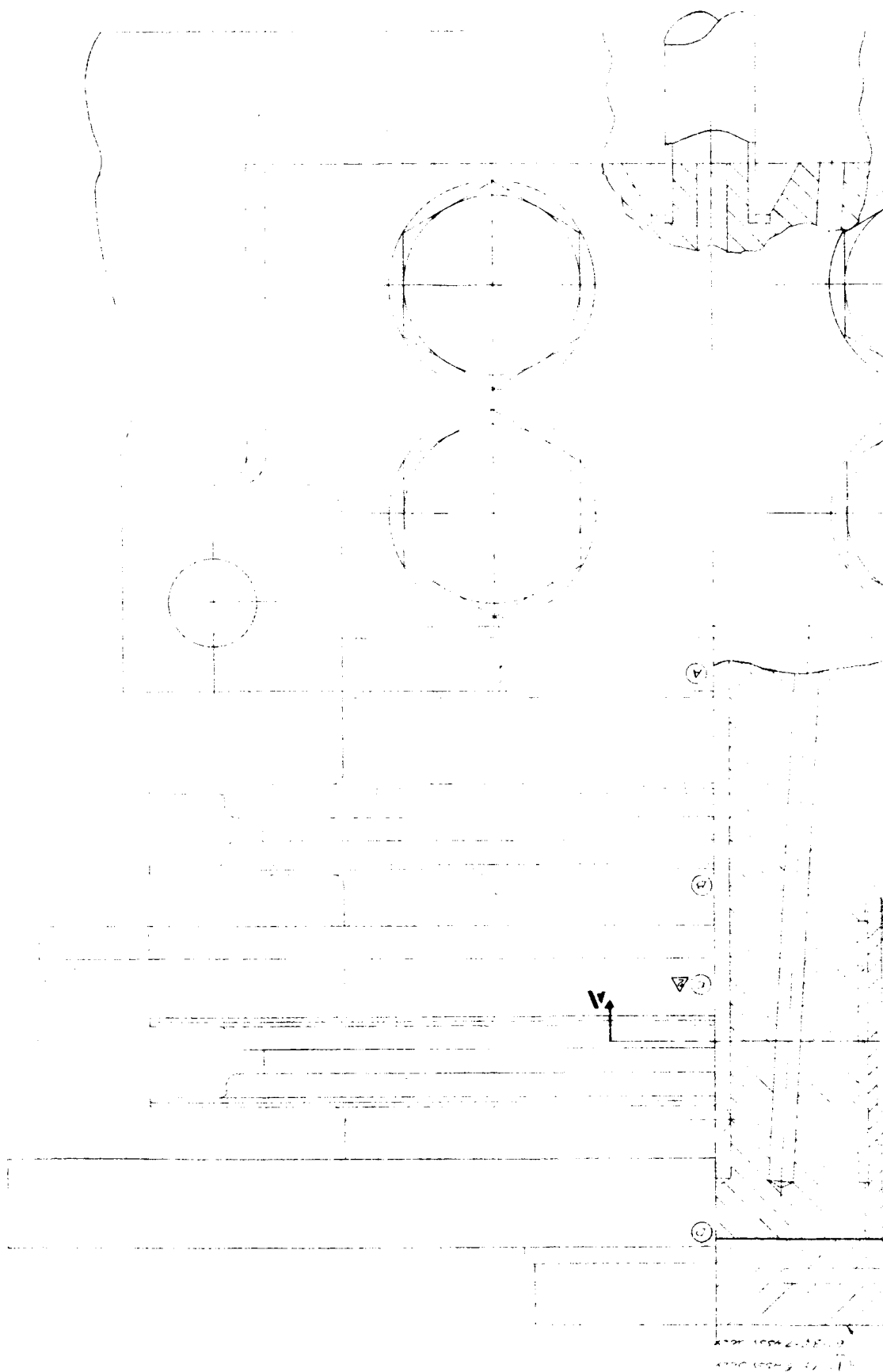
the guard ring and collector. Three separate sets of guard ring-collector assemblies will be fabricated. One set will be constructed completely of molybdenum, one set will have a tantalum button brazed to the surface of the molybdenum collector barrel, and the third will have a rhenium button brazed to the surface of the molybdenum collector barrel.

Three specially machined screws will be used primarily to position the guard ring vertically with respect to the collector. The position of the screw is shown in section A-A of Fig. 2-10. These screws will be fabricated from molybdenum. The secondary purpose of the screws is to mechanically fasten the guard ring and collector at a common point so that the thermal expansion of both members will be identical during operation of the vehicle.

The vehicle utilizes a prefabricated concept. As many subassemblies as possible are to be preassembled before being united in the final variable parameter vehicle assembly. First, the ceramics are brazed to the flat niobium flanges shown in Fig. 2-10. In separate operations, the four flared niobium flanges are brazed to the emitter plate, guard-ring plate, and collector subassemblies. The subassemblies are stacked in a jig, sandwiching the ceramic seals, and four heli-arc welds are made around the circumference of the vehicle. This seals the device and forms the bellows. In common electron device fabrication practice, metal-ceramic seals are brazed in position on the device. This results in the loss of the entire vehicle if the seals are not vacuum tight after brazing. In this design, the metal-ceramic seals are prebrazed and leak tested, and final assembly of the vehicle is then completed as described above by heli-arc welding. Heli-arc welded joints are inherently much safer joints to make successfully on one-of-a-kind assemblies. This process eliminates the establishment of electron beam weld schedules or high temperature braze schedules involving multiple steps incorporating different thermal masses for each successive joint.



FIG. 2-10 EMISSION VEHICLE LAYOUT





To date, the major fabrication effort has been directed toward the development of a single-convolution refractory-metal bellows. A bellows was fabricated and it consists of two niobium flanges welded together at the outside diameter, which is 1.500 inches. The bellows was measured to have an excursion greater than 0.040 inch and, in the unannealed state, required an excursion force of 1.6 lbs/mil. The successful fabrication of thin-walled refractory-metal bellows is seen to be mainly dependent upon the effective chill-blocking of the welding samples. Without chill blocks, the thin (0.010 inch) sheets of refractory metal used in the bellows became greatly distorted during the welding process due to differential thermal stress in the welded material. After welding the bellows was annealed at 1500°C for 10 minutes to stress-relieve the bellows material. Following the anneal, the excursion force was measured to be 0.58 lbs/mil. The bellows assembly was then placed on cycle life test. The niobium bellows assembly successfully completed 3500 cycles at room temperature with a 25 mil excursion without any signs of metal fatigue. At this time, the excursion force had increased to 0.64 lbs/mil. This increase is probably a result of work hardening of the material. At 8000 cycles, the bellows ruptured due to work hardening. EOS feels it has proven the feasibility of utilizing welded niobium bellows for expansion members. Niobium was chosen for the bellows material due to the pure state in which niobium may be obtained (99.9 percent). It has a very high melting point (2415°C) resulting in no contamination of the vehicle during high-temperature operation.

### 2.1.3 Parametric Measurements

Figure 2-11 is a schematic of the emission vehicle test circuit. The power supply shown in the figure is utilized to bias the emission vehicle during those periods of operation when the voltage is swept into the power consuming quadrant. This bias is required at low emitter temperatures and large interelectrode spacings where an applied voltage is needed to draw saturated emission from the emitter. The equalizing load resistor is required to balance the voltage difference between the collector and guard ring.

The basic components of the constant current-voltage sweep load are shown in Fig. 2-12. The electronic load is a voltage-regulated power consuming device. It has a nominal regulating capability of 2.6 mV at currents ranging from 1 to 50 amps. Its maximum average current capability is 200 amps and has saturation characteristics of 75 mV at 100 amps. Its regulating range is from 0.25 V to 1.4 V. The sweeping circuitry employs the 60-cycle sweep and sweeps down to a nominal 0.10 V (at high currents). Peak currents to 400 amps will be within safe operating limits of the load. The maximum voltage that can be applied to the load transistors is 5 volts. The load employs extremely low-saturation-resistance germanium transistors.

### 2.2 Materials Process Study

The objective of this study is to generate a processing schedule for the materials selected as electrodes in the variable parameter vehicle or high-performance converters. The process schedule will include a detailed chemical cleaning treatment and vacuum outgassing procedure for achieving uncontaminated, stable electrode surfaces.

The emitting electrode in a high-performance thermionic converter operates at a temperature of  $2000^{\circ}\text{K}$ , which may result in excessive grain growth and unstable emission if the emitter surface has not been previously heat treated in a manner sufficient to establish a stable grain structure. The core of the problem, therefore, is to determine a surface finishing and vacuum outgassing schedule which

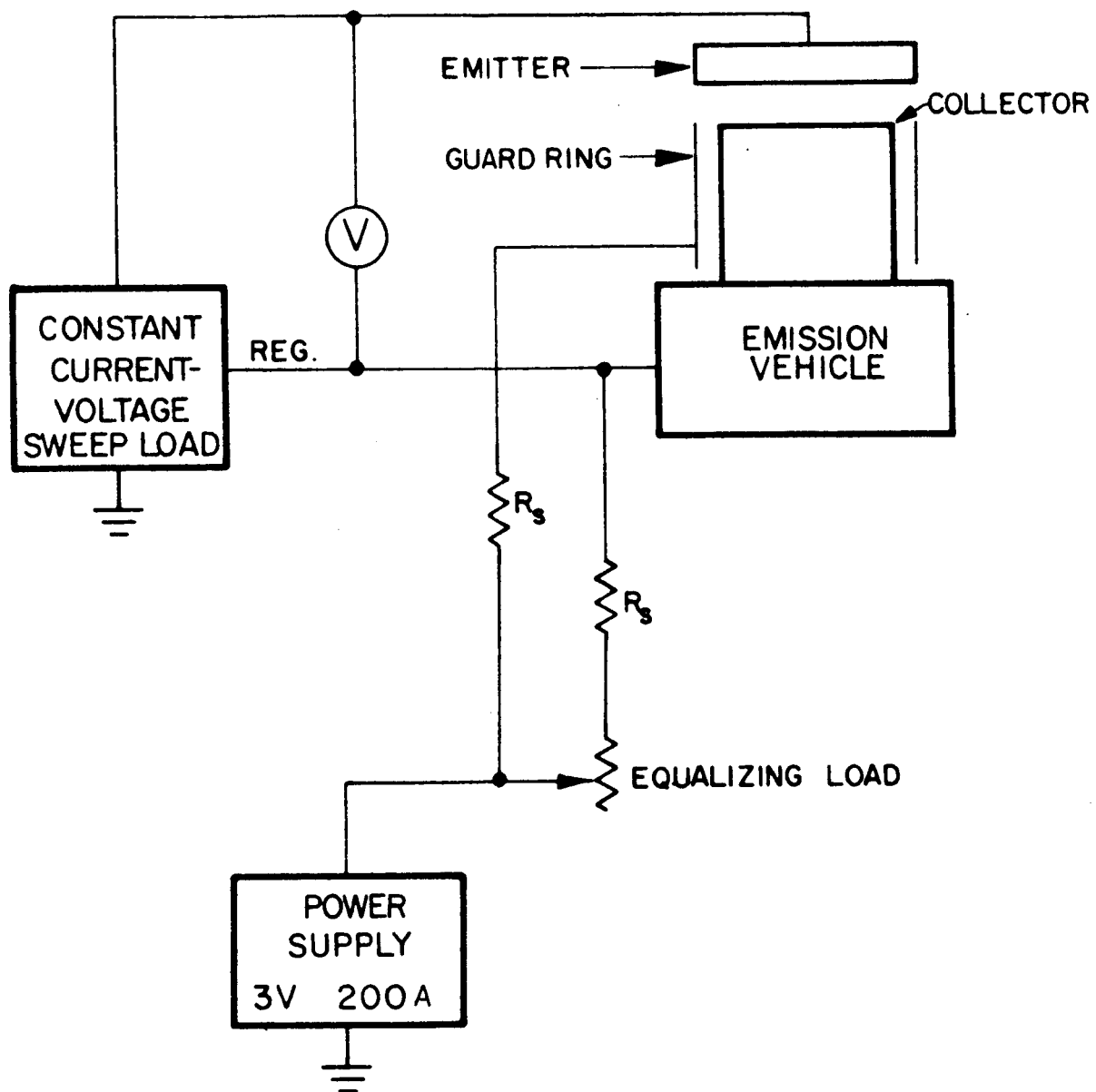


FIG. 2-11 EMISSION VEHICLE TEST SCHEMATIC

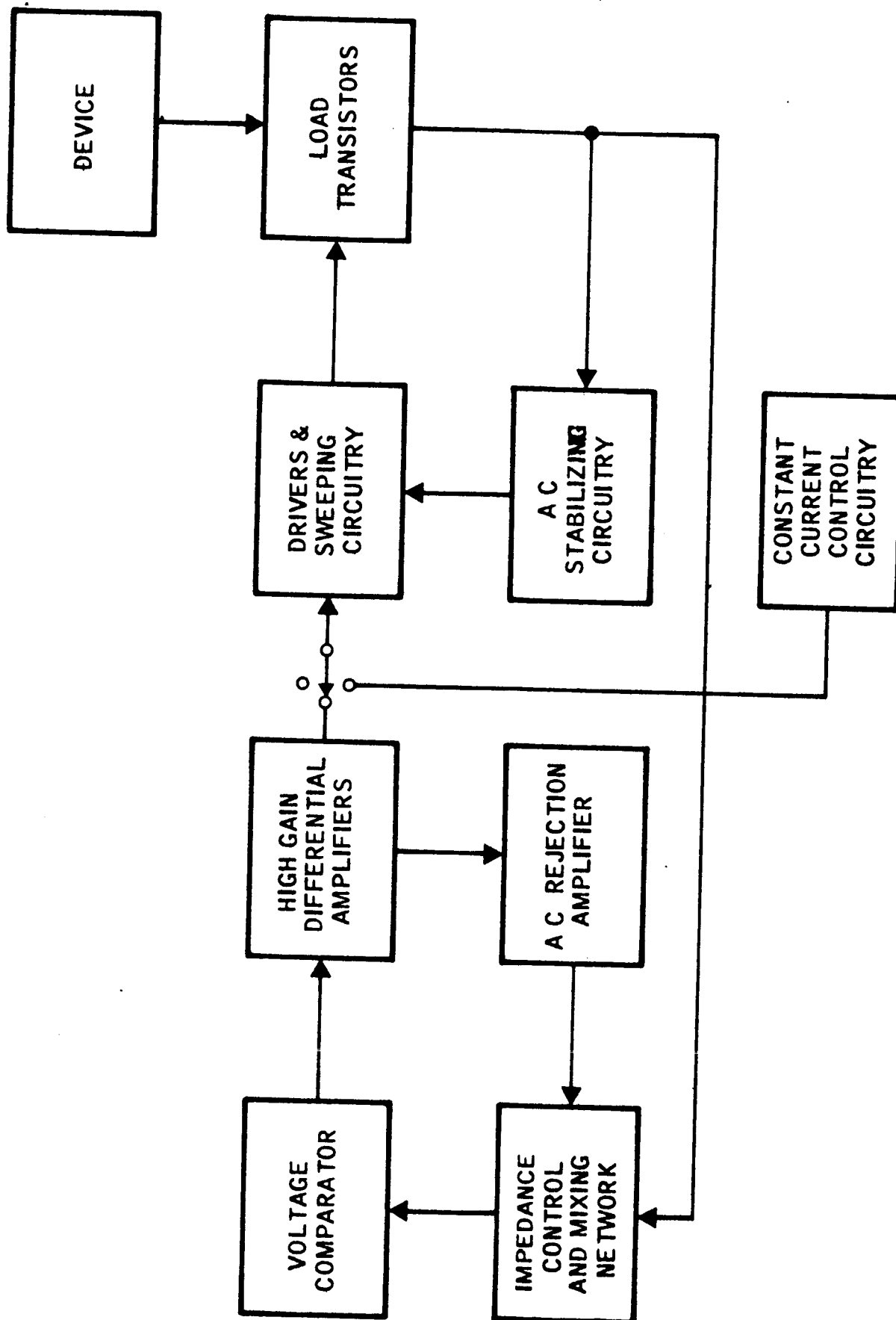


FIG. 2-12 CONSTANT CURRENT-VOLTAGE SWEEP LOAD

will not only remove gaseous and high vapor pressure elements, but which will also set the grain structure of the emitter such that subsequent operation for an extended length of time (i.e., much greater than 100 hours) at a temperature of 2000°K will not effect changes in the emitter surface structure.

The materials selected for this process study are Rembar high-purity plate-stock rhenium and NRC high-purity rod-stock tantalum. The following paragraphs discuss the analyses of the stock in the "as received" condition, the sample preparation, vacuum outgassing schedules, and preliminary results of the surface stability.

#### 2.2.1 Analysis of Stock

As a starting point for the processing study, a detailed mill history for each material has been requested from the supplier. Upon receipt of each material, a spectrographic analysis was performed by the Materials Testing Laboratory (MTL), a Division of the Magnaflux Corporation, to provide comparison with the supplier's certification of purity. Table 2-III and 2-IV present the data obtained from the MTL tests.

The analyses differ significantly on the amount of impurities present in each sample. The differences are due to the method of testing as well as to the interpretation of the spectra, the latter may account for impurity values which were optimistically reported to range from 1 to 10 ppm.

#### 2.2.2 Sample Preparation

Three bar-stock tantalum disks of 0.800 inch diameter and 0.200 inch thickness were machined to achieve a tolerance of 0.0001 inch flatness and 0.0001 inch perpendicularity without the use of oil lubricants. Such tolerances will be required in the variable parameter vehicle study for accurate measurements of thermionic power output at 0.0005 inch interelectrode spacings. The actual machined tolerances were: Flatness to within 30 millionths of an inch and perpendicularity or "squareness" to within 19 millionths of an inch; both as measured

TABLE 2-IIIA

## NRC REPORT ON ANALYSIS OF HIGH-PURITY TANTALUM BAR STOCK

Tantalum	Remainder (99.87 percent)
Chromium	0.0001 percent*
Copper	0.0001 percent*
Iron	0.0005 percent
Molybdenum	0.0048 percent
Tungsten	0.01 percent
Aluminum	0.0001 percent
Columbium	0.0095 percent
Total Other Elements	0.106 percent*

\*Less than

TABLE 2-IIIB

MATERIALS TESTING LABORATORIES REPORT ON SPECTROGRAPHIC  
ANALYSIS (SEMI-QUANTITATIVE) OF HIGH-PURITY TANTALUM BAR STOCK

Tantalum	Remainder (99.62 percent)
Chromium	0.003 percent
Copper	0.001 percent
Iron	0.01 percent
Molybdenum	0.01 percent
Tungsten	0.10 percent*
Aluminum	0.0001 percent
Calcium	0.001 percent
Columbium	0.10 percent*
Total Other Elements	0.15 percent

\*Less than

TABLE 2-IVA  
REMBAR REPORT ON ANALYSIS OF HIGH-PURITY RHENIUM PLATE STOCK

Rhenium	Remainder (99.99 percent)
Aluminum	0.0001 percent
Nickel	0.0005 percent
Copper	0.0001 percent
Gold	0.0042 percent
Manganese	0.0001 percent
Silicon	0.0001 percent
Total Other Elements	Not Detected

TABLE 2-IVB  
MATERIALS TESTING LABORATORIES REPORT ON SPECTROGRAPHIC ANALYSIS  
(SEMI-QUANTITATIVE) OF HIGH-PURITY RHENIUM PLATE STOCK

Rhenium	Remainder (99.96 percent)
Calcium	0.005 percent
Titanium	0.002 percent
Molybdenum	0.01 percent
Aluminum	0.002 percent
Magnesium	0.003 percent
Chromium	0.01 percent
Silicon	0.007 percent
Others	Not Detected

by the EOS Quality Assurance Laboratory on a Pratt & Whitney electronic micrometer capable of determining accuracy to ten millionths of an inch. A profilometer reading indicated that the surface smoothness on the sample surfaces ranged from 30 to less than 16 micro-inches.

The samples were chemically cleaned in accordance with the procedure described in Appendix A and were stored in dustproof, moisture-proof containers until required for vacuum outgassing.

#### 2.2.3 Vacuum Outgassing Schedules for Tantalum

The tantalum samples which were machined and chemically cleaned as described in the previous paragraphs were mounted in refractory metal firing stands for electron bombardment heating in a vacuum pumped vacuum environment. The tantalum firing stands are fitted with high-purity, vacuum-fired tantalum tubes which support the samples. Tantalum was purposely selected as the support material to prevent the formation of eutectics or the diffusion of metal support impurities into the tantalum sample during the high-temperature firing operation.

As a starting point for this investigation, an outgassing schedule of 2100°C for 2 hours was selected for the first sample. The second sample was outgassed at 2250°C for 2 hours and the third sample at 2410°C for 2 hours. All temperature measurements were made by viewing an 8:1 hohlraum with a calibrated micro-optical pyrometer. The sample surfaces were subsequently examined on a Zeiss metallograph. Individual grains were marked by a microhardness tester and photographed without metallographic preparation such as etching or polishing. The samples were returned for 100-hour operation at 1735°C.

#### 2.2.4 Surface Stability Examination

Figures 2-13 and 2-14 are comparison photographs of samples outgassed at 2100°C and 2250°C, respectively, and then operated at 1735°C for 100 hours. The circular grooves that appear in the photographs of the sample surface are machining marks. The samples were not lapped or polished since tantalum becomes contaminated with embedded

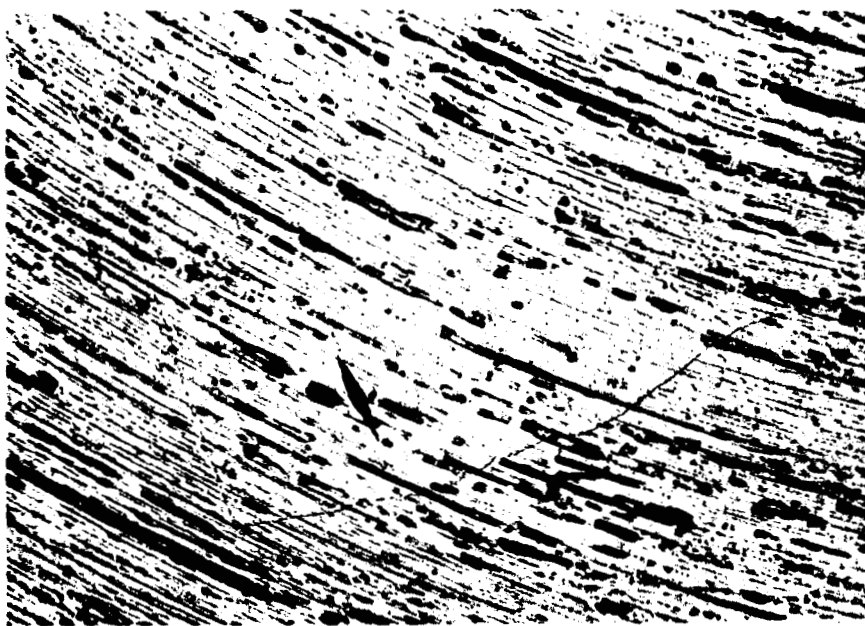


FIG. 2-13a TANTALUM PROCESS SAMPLE VACUUM-FIRED AT 2100°C FOR 2 HOURS IN A VAC-ION PUMPED ATMOSPHERE OF  $1 \times 10^{-7}$  torr (X100)

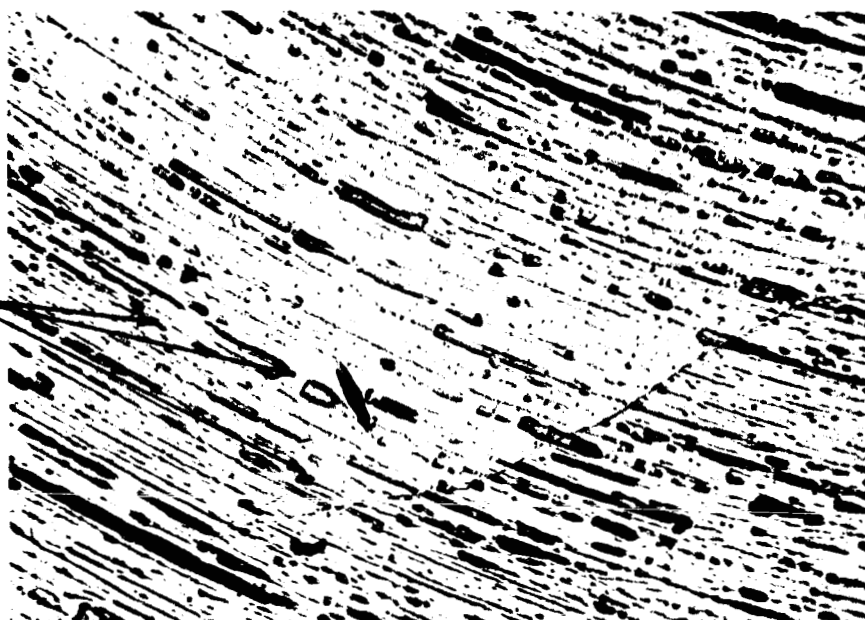


FIG. 2-13b SAME SAMPLE AFTER OPERATION AT 1735°C FOR 100 HOURS AT  $5 \times 10^{-8}$  torr (X100)

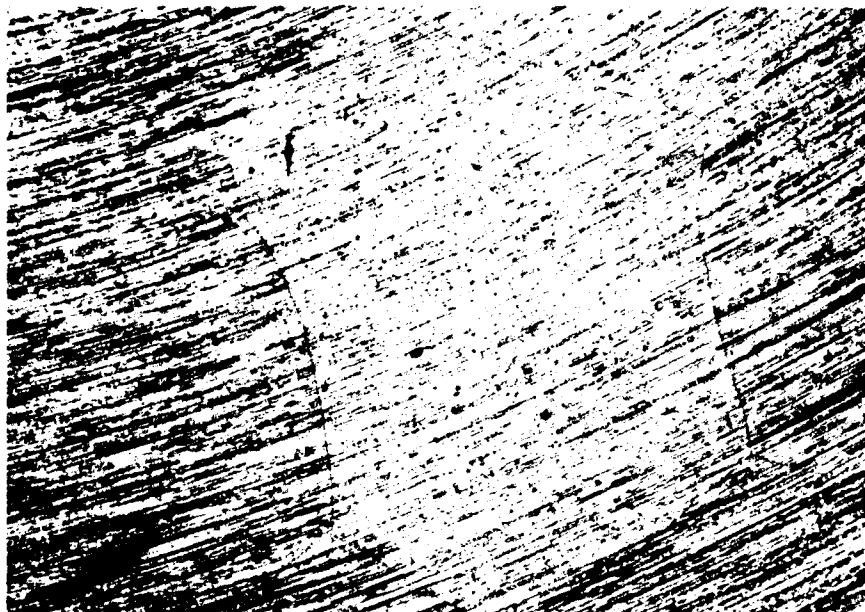


FIG. 2-14a TANTALUM PROCESS SAMPLE VACUUM-FIRED AT 2250°C FOR 2 HOURS IN A VAC-ION PUMPED ENVIRONMENT OF  $4 \times 10^{-7}$  torr (X50)

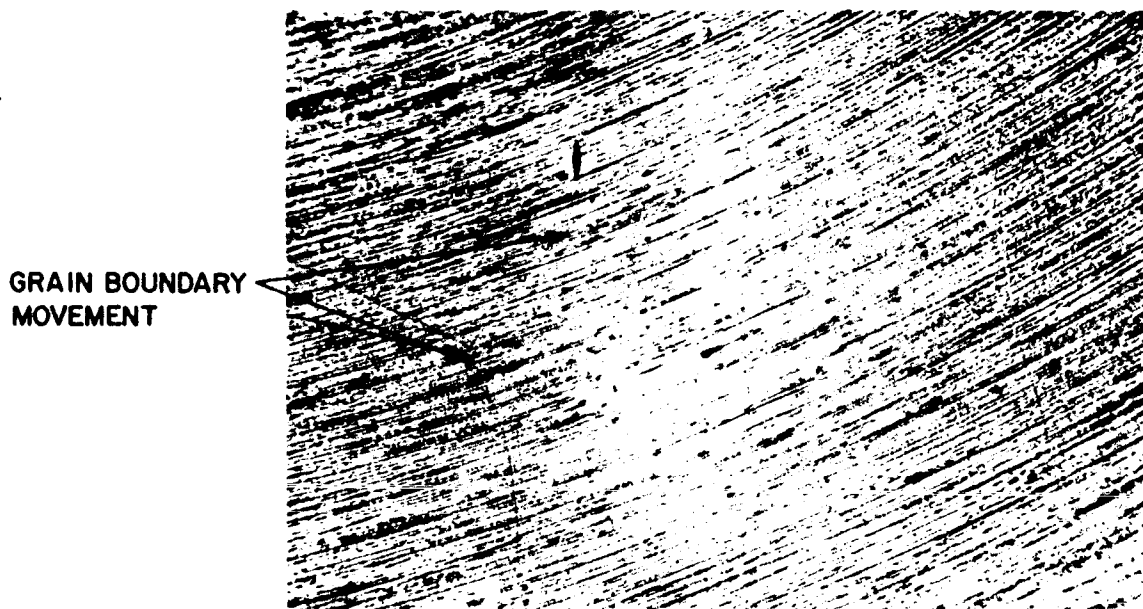


FIG. 2-14b SAME SAMPLE AFTER OPERATION AT 1735°C FOR 100 HOURS IN A VAC-ION PUMPED ENVIRONMENT OF  $5 \times 10^{-8}$  torr (X50)

particles acquired from lapping and polishing operations. On both sets of photographs, there is ample evidence of grain boundary movement which indicates that the processing schedule was not sufficient to produce a stable electrode surface.

The 2410°C outgas sample is presently being examined for surface stability.

### 3. COLLECTOR STUDY AND SECONDARY EXPERIMENTS

#### 3.1 Collector Heat Transfer Study

An investigation has been started to reduce the collector-barrel temperature drop in a high-performance converter. Two approaches are being considered: (1) to optimize the L/A ratio of the barrel section and still retain a realistic geometry capable of fabrication, and (2) to increase the thermal conductivity of the barrel section by inserting a material having a higher conductivity than molybdenum in the heat transfer path.

These two approaches are presently being developed and are reported on in the following paragraphs.

##### 3.1.1 Thermal Design Curves for Non-Composite Collector

The collector heat load in a thermionic converter may be calculated by summing the individual contributions of electron heating, net radiation heat transfer from emitter to collector, and the conduction heat transfer from cesium atoms. The first term, electron heating, may be written as:

$$Q_{eh} = I \left( \phi_{coll} + \frac{\epsilon k T_{pl}}{e} \right) \quad (11)$$

since the drift electrons dissipate the energy acquired by falling through the potential of the collector work function plus random potential energy in the plasma. The value of  $\epsilon$  is chosen such that  $1.3 \leq \epsilon \leq 1.5$  depending on the plasma electron energy distribution.  $T_{pl}$  is selected to be  $6000^\circ\text{K}$ . The collector work of cesium on molybdenum,  $\phi_{coll}$ , has been measured at 1.55ev. Therefore, the electron heating contribution,  $Q_{eh}$ , is written as

$Q_{eh} = I(2.2)$ , where  $I$  is the drift current or external circuit current from an operating current.

The second term, net radiation heat transfer from emitter to collector, is written as

$$Q_{\text{rad}} = \epsilon_{\text{eff}} \sigma (T_{\text{em}}^4 - T_{\text{coll}}^4) \quad (12)$$

where  $\epsilon_{\text{eff}}$  is the effective emissivity of electrode system.

$$\epsilon_{\text{eff}} = \frac{1}{\frac{1}{\epsilon_{\text{em}}} + \frac{1}{\epsilon_{\text{coll}}} - 1} \quad (13)$$

The net radiation heat transfer for  $T_{\text{em}} = 2,000^\circ\text{K}$ ,  $T_{\text{coll}} \approx 1,100^\circ\text{K}$ ,  $\epsilon_{\text{em}} = 0.3$ , and  $\epsilon_{\text{coll}} = 0.25$ , and for two square centimeters of area is:

$$Q_{\text{rad}} = 26 \text{ watts}$$

The last term, cesium conduction, has been experimentally determined (Ref. 5) to be:

$$Q_{\text{cs}} = 16 \text{ watts}$$

The sum of these contributions are substituted into the classical heat conduction equation and  $\Delta T$ 's (temperature differences between collector surfaces and collector roots) are computed for various converter current loads. Figure 3-1 is a plot of the  $\Delta T$  as a function of the converter current with the collector band L/A ratio as the parameter. The cross-sectional area, A, is fixed at  $1.9 \text{ cm}^2$ . Consequently, at the design point of 50 amperes of current flow, a collector barrel length of 0.6 inch results in a temperature drop of  $108^\circ\text{C}$ . It is important to note that any slotted or stepped portions of the collector barrel may not be considered as a series connection of thermal impedance since the lines of heat flux are disturbed and do permit a simple, linear treatment.

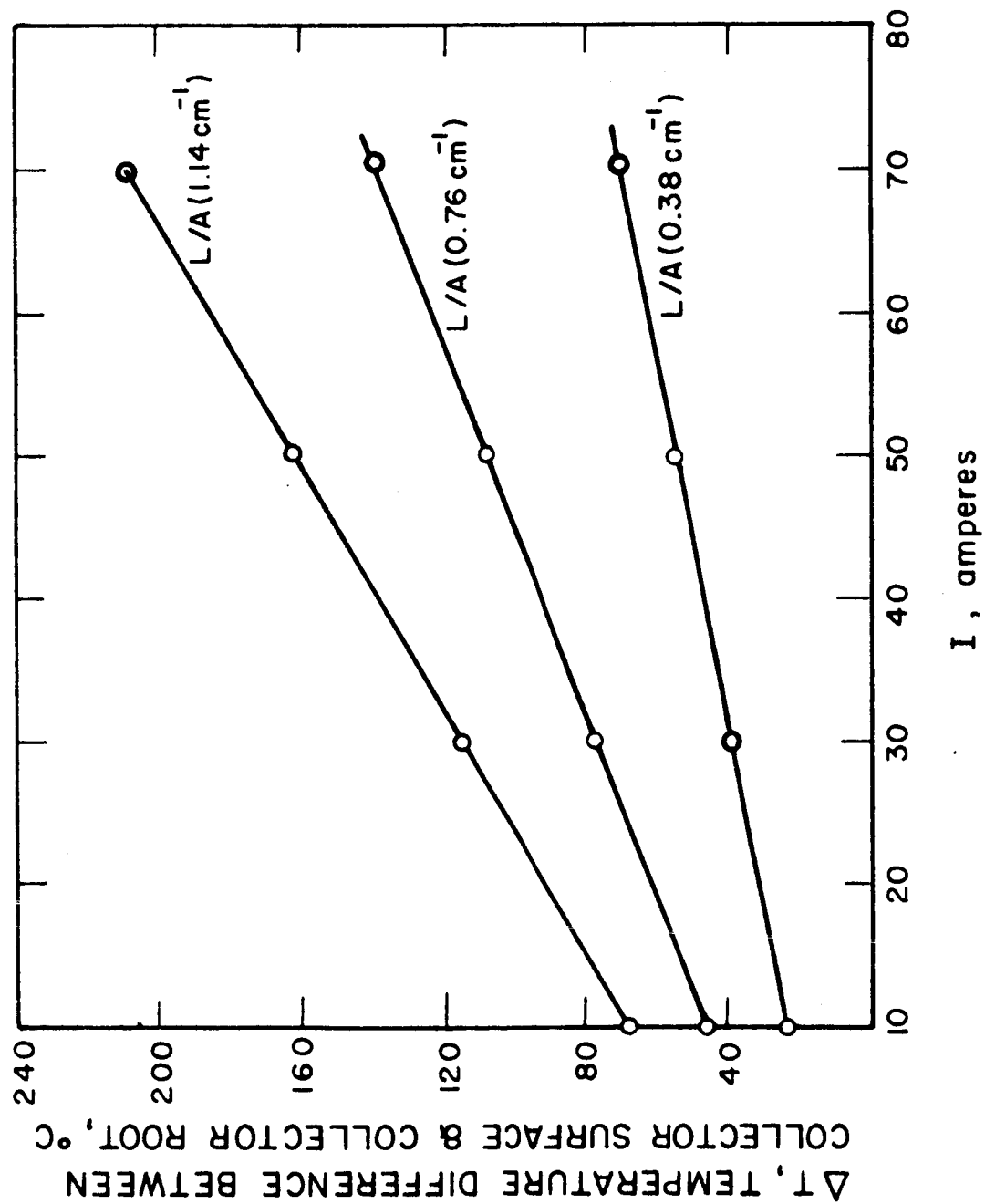


FIG. 3-1 THERMAL DESIGN CURVES FOR NONCOMPOSITE COLLECTOR

### 3.1.2 Composite Collector Thermal Experiment and Metallographic Analyses

The concept of increasing the effective thermal conductivity of a molybdenum collector barrel by inserting copper in the heat transfer path depends upon achieving a void-free, metallurgical bond between copper and molybdenum. A composite collector of molybdenum and copper was prepared as shown in Fig. 3-2. The assembly was brought to the melting point of copper (i.e.,  $1,086^{\circ}\text{C}$ ) and was prepared for subsequent thermal cycle testing. The expansion mismatch between copper and molybdenum is so severe that it is reasonable to suspect that continued cycling would rupture any bond resulting from the melting operation; or worse, the collector surface might warp out of tolerance and make it useless for converter application.

The composite structure was thermally cycled 60 times from  $800^{\circ}\text{C}$  -  $200^{\circ}\text{C}$  without change in the  $\Delta T$  from top to bottom. After operation, the collector surface and barrel dimensions were measured and were found to be within 0.0001 inch of the original dimensions. Figure 3-3(a) and Fig. 3-3(b) are photomicrographs of the molybdenum-copper bond. There appears to be no void structure at the interface, no evidence of shear cracks and no formation of a brittle intermetallic compound. This type of bond is capable of high heat transfer rates without a large temperature drop, thus permitting the copper to effectively reduce the thermal conductivity of the collector barrel.

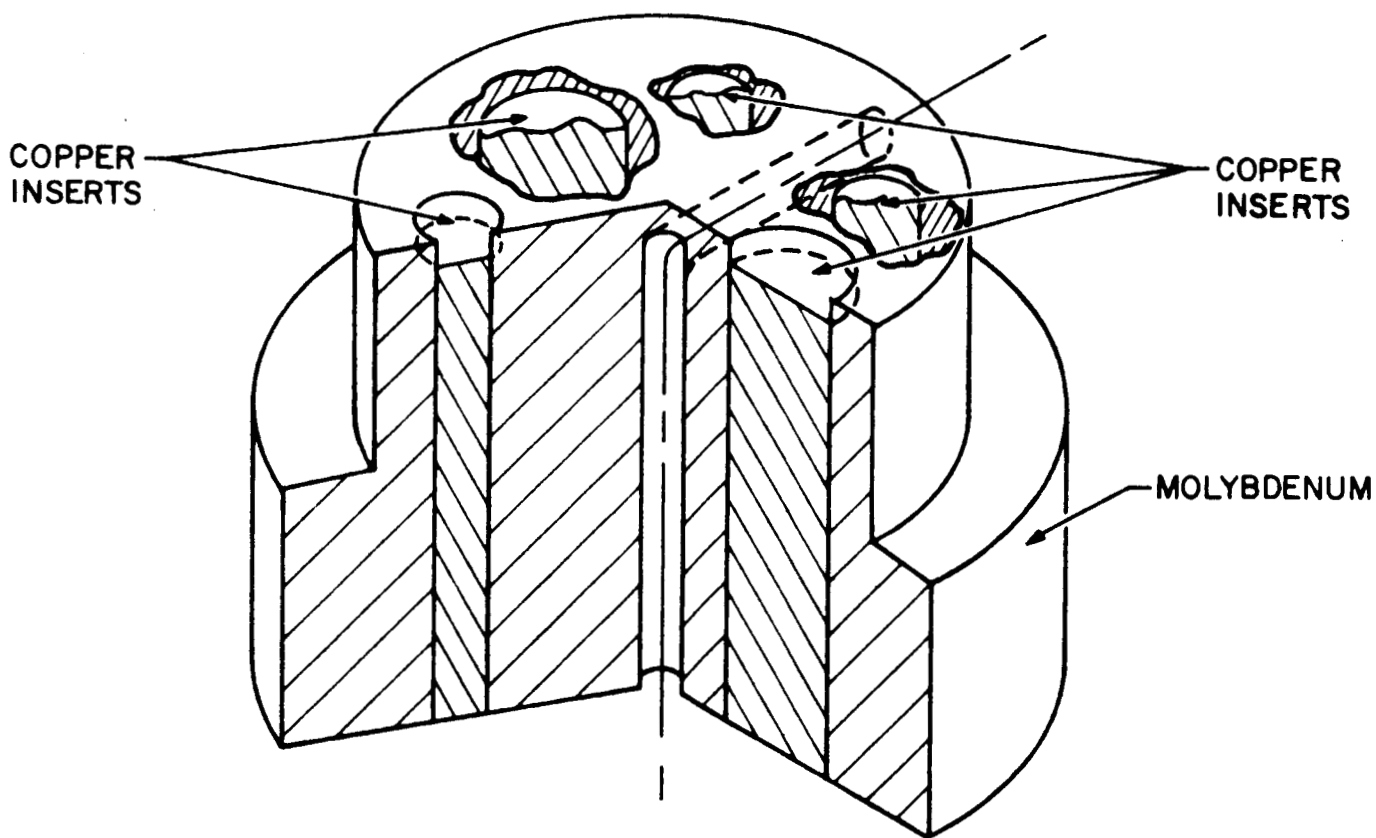


FIG. 3-2 COMPOSITE COLLECTOR, MOLYBDENUM AND COPPER

Cu

Mo

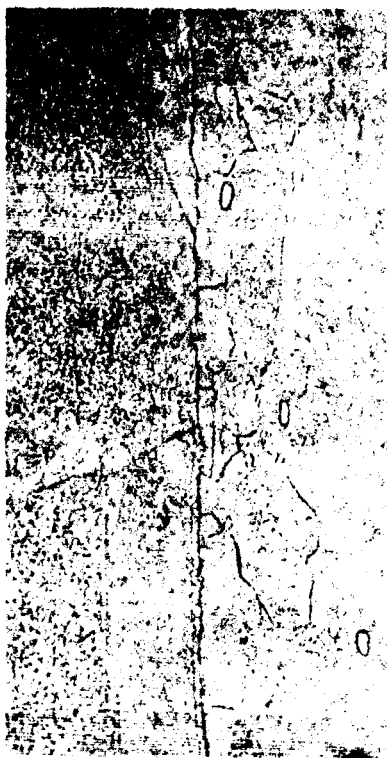


FIG. 3-3a

MICROGRAPH OF MOLYBDENUM-COPPER  
INTERFACE (X500)

Cu

Mo



FIG. 3-3b

MICROGRAPH OF MOLYBDENUM-COPPER  
INTERFACE NEAREST COLLECTOR  
SURFACE (X500)

### 3.2 Radiator Heat Rejection

#### 3.2.1 Rokide "C" Investigation

Three separate studies are being conducted with the goal of improving the radiator heat rejection efficiency of thermionic converters.

The first study is concerned with the long term stability of Rokide "C" coatings on two radiator materials, molybdenum and copper. The coating stability is being investigated in a temperature range appropriate to converter radiators (i.e. approximately 600°C), in a vac-ion pumped environment at  $10^{-8}$  mm Hg and for periods of time extending to 500 hours. In addition to the stability of the Rokide coating, experiments have been conducted to determine the value of its total emissivity. As a part of the study, the parameters for applying Rokide have been documented in detail to ensure process control.

The second study is a mathematical analysis of a constant-temperature-gradient radiator surface which has been claimed to be an optimum weight configuration (Ref. 1). The analysis supplies expressions for fin thickness and total radiant heat transfer. The EOS production prototype converter utilizing an integral collector-radiator is reviewed employing the analytic results.

The third study investigates the feasibility of using a nonintegral collector-radiator to decrease the collector  $\Delta T$  at high heat transfer rates while maintaining mechanical rigidity and minimum weight. The parts have been fabricated for the experiment and testing will start immediately.

##### 3.2.1.1 Stability of Rokide "C" Coated Molybdenum

A molybdenum rod was coated with Rokide "C", instrumented with chromel-alumel thermocouples for temperature measurement, and mounted on a refractory fixture for extended operation at temperatures of 600°C. Figure 3-4 is a sketch of coating specimen showing the coated and uncoated portions and the thermocouple locations. Measurements of the rod diameter were taken before plasma spraying and were compared with the measurements of the rod diameter

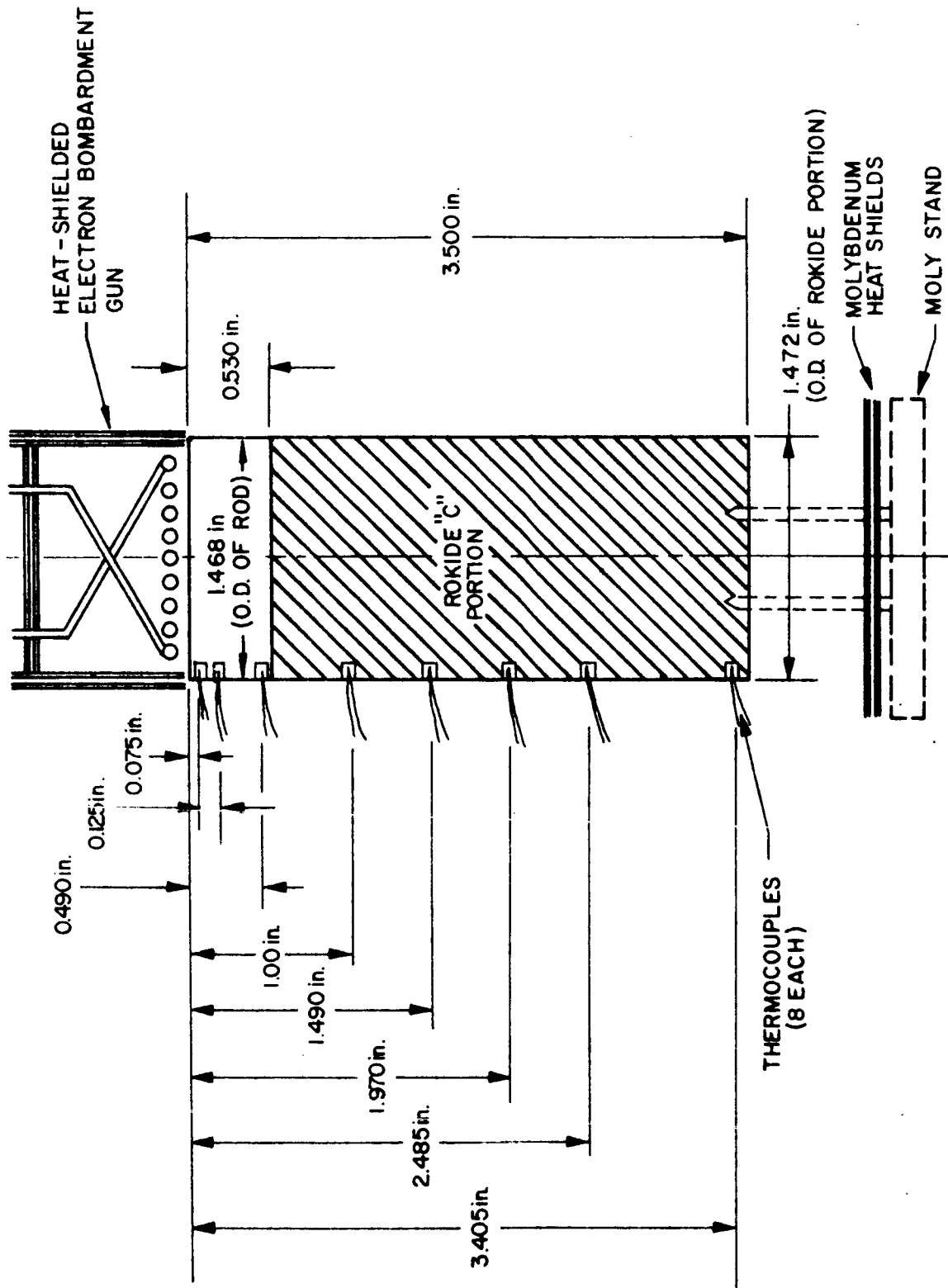


FIG. 3-4 THERMOCOUPLE LOCATIONS AND SAMPLE DIMENSIONS OF MOLYBDENUM-ROKIDE "C" EXPERIMENT

after plasma spraying to determine the Rokide thickness. The thickness of Rokide was determined to be  $0.0025 \pm 0.005$  inch. To provide a reproducible coating schedule, close documentation of the plasma spraying procedure was maintained.

The sample was heated to  $600^{\circ}\text{C}$  by electron bombardment in a vac-ion pumped environment of lower than  $5 \times 10^{-8}$  mm Hg for 500 hours. The physical appearance of the coating did not change during this period of time. There was no peeling, blistering, or cracking of the Rokide even though a number of rapid thermal cycles (greater than 30) occurred during test. Figure 3-5 is a photograph of the sample after test. Ceramic-sheathed couples facing the Rokide showed no evidence of discoloration which would be indicative of coating deterioration. The electron bombardment input power remained constant (as did the sample temperature distribution) during the 500 hours of operation.

The bell jar used for this test was calibrated against a standard tungsten ribbon filament lamp before any testing of the sample. It was again calibrated at 210 hours and again at 492 hours. This was done to determine what increase in light transmission losses could be expected due to prolonged periods of testing. After 500 hours of operation, there was only a slightly noticeable coating on the test bell jar. Table 3-I shows the increase in transmission losses at three different times during the test run. There is no evidence that the slight jar discoloration was due to heating of the Rokide sample. In fact, it may have been caused by the evolution of material from some of the stainless steel fittings inside the bell jar, which normally operate at  $200\text{-}300^{\circ}\text{C}$  during test.

#### 3.2.1.2 Rokide "C" Emissivity (Total) Measurements

The Rokide emissivity was obtained from periodic cool-down curves which were taken during the 500-hour stability investigation. Using handbook data for the specific heat of molybdenum, and correcting for the area not coated with Rokide, the



FIG. 3-5 ROKIDE "C"-COATED MOLYBDENUM SAMPLE AFTER 500 HOURS OF OPERATION (Note: the alumina tubes facing the Rokide coating are not discolored)

TABLE 3-I  
 BELL-JAR TRANSMISSION LOSS AS A FUNCTION OF TEST TIME  
 DURING ROKIDE "C" STABILITY EXPERIMENT

<u>Increase in Transmission Loss (Bell-Jar Surrounding Std. Lamp)</u>			<u>Test Time (Hours)</u>
<u>1000°C</u>	<u>1600°C</u>	<u>1700°C</u>	
0°C	0°C	0°C	0 hours
3°C	10°C	10°C	210 hours
4°C	15°C	19°C	492 (final)

emissivity may be calculated from the temperature and time measurements during cool-down.

The heat balance is established as follows:  
The heat lost by radiation must be equal to the change in heat energy of the sample, that is:

$$a\epsilon\sigma T^4 = -mC_p \frac{\Delta T}{\Delta t} \quad (14)$$

where:  $a$  = radiating area in square centimeters  
 $\epsilon$  = emissivity of the radiating surface  
 $\sigma$  = Stefan-Boltzmann constant,  $1.354 \times 10^{-12} \text{ cal cm}^{-2} \text{ } ^\circ\text{K}^{-4} \text{ sec}^{-1}$   
 $T$  = radiating temperature, degrees Kelvin  
 $m$  = mass of sample in grams  
 $C_p$  = specific heat constant in  $\text{cal gm}^{-1} \text{ } ^\circ\text{K}^{-1}$   
 $\Delta T$  = change in temperature in degrees Kelvin  
 $\Delta t$  = change in time in seconds

For this investigation,  $a\epsilon\sigma T^4$  must be separated into the sum of two radiating losses, one from the molybdenum surface and one from the Rokide surface. The emissivity of the Rokide surface is then expressed as:

$$\epsilon_R = \frac{-mC_p \frac{\Delta T}{\Delta t} - (A_m \epsilon_m \sigma T_m^4)}{A_R \sigma T_R^4} \quad (15)$$

The cool-down curves of the Rokide-molybdenum sample are shown in Fig. 3-6. The identical character of the initial and final cool-down curves is further evidence of the coating stability. The technique of obtaining the cooling curves is as follows: (1) a steady-state temperature of the sample is achieved, (2) all power input is immediately cut-off, (3) the time-versus-temperature curve is automatically recorded by a sensitive X-Y plotter or strip chart recorder. Within 8 seconds the temperature of the unRokided portion

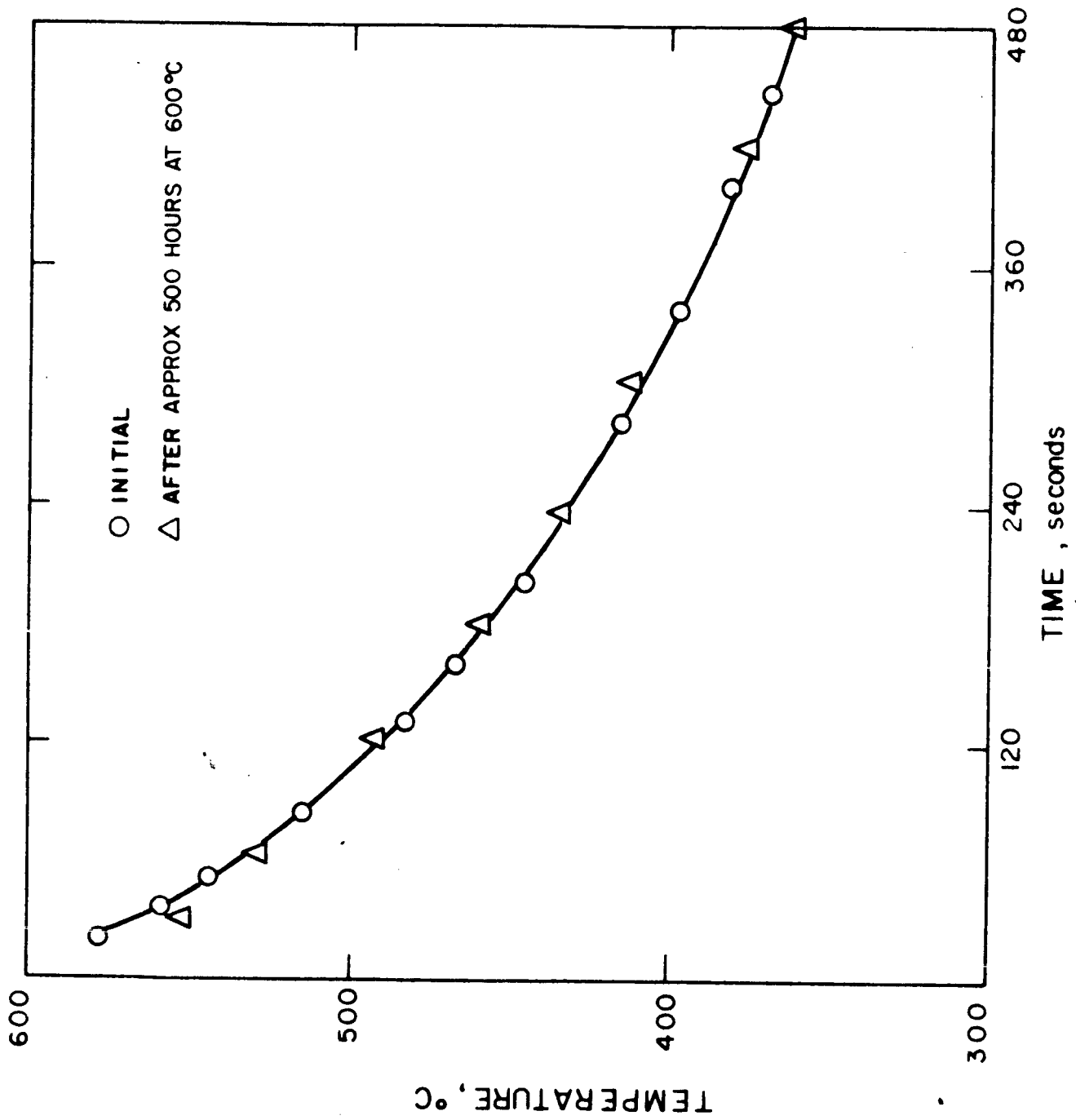


FIG. 3-6 COOLDOWN CURVES OF ROKIDE "C"-COATED MOLYBDENUM SAMPLE

( $T_m$ ) and the Rokided portion ( $T_R$ ) are within thermocouple error and consequently are assigned the same value ( $647^\circ\text{K}$ ) for the calculations. From cool-down data such as shown in Fig. 3-6, the value for the emissivity of the Rokide is computed as follows:

$$\epsilon_R = \frac{(986.5 \text{ g}) \left( \frac{0.065 \text{ cal}}{\text{g}^\circ\text{K}} \right) \left( \frac{47^\circ\text{K}}{200 \text{ sec}} \right) - (36 \text{ cm}^2)(0.2) \left( 1.354 \frac{\text{cal}}{\text{cm}^2 \text{ deg}^4 \text{ sec}} \right) (10^{-12}) (643^\circ\text{K})^4}{(88 \text{ cm}^2)(1.354) \left( \frac{10^{-12} \text{ cal}}{\text{cm}^2 \text{ deg}^4 \text{ sec}} \right) (643^\circ\text{K})^4}$$

where:  $\Delta t = t_2 - t_1 = 480 \text{ sec} - 280 \text{ sec} = 200 \text{ sec}$

$$T^4 \cong T_{\text{ave}}^4 = (643^\circ\text{K})^4$$

$$C_p = 0.065 \text{ cal} \cdot \text{gm}^{-1} \cdot ^\circ\text{K}^{-1}$$

$$\epsilon_m = 0.2$$

$A_m, m, A_r$  are measured quantities

$$\epsilon_R = \frac{17.65 - 1.65}{20.2} = 0.79$$

This method of approximation leads to a small error since only average values for the temperature are used. A more exact solution is as follows:

$$(A_{\text{Rok}} \epsilon_{\text{Rok}} + A_{\text{mo}} \epsilon_{\text{mo}}) \int_{t_i}^{t_f} dt = \frac{-mC_p}{\sigma} \int_{T_i}^{T_f} \frac{dT}{T^4} \quad (16)$$

$C_p \neq f(T)$  a good assumption over temperature range of analysis (Ref. 2)

$\epsilon_{\text{Rok}}, \epsilon_{\text{mo}} \neq g(T)$  a good assumption over temperature range of analysis (Ref. 2)

$$(A_R \epsilon_R + \epsilon_{\text{mo}} A_{\text{mo}})(t_f - t_i) = \frac{+MC_p}{3\sigma} \left[ \frac{1}{T_f^3} - \frac{1}{T_i^3} \right]$$

From the data in Fig. 3-6:

$$\begin{aligned} t_f &= 480 \text{ sec} & T_f &= 633^\circ\text{K} \\ t_i &= 60 \text{ sec} & T_i &= 803^\circ\text{K} \\ \epsilon_{\text{mo}} &= 0.2 \text{ (Ref. 2)} \end{aligned}$$

$$\left\{ 88 \text{ cm}^2 \epsilon_R + (0.2)(36) \text{ cm}^2 \right\} (480 - 60) = \frac{+ 986 \times \frac{0.066}{^\circ\text{K}}}{\frac{(3)(1.354)(10^{-12})}{\text{cm}^2 \text{ deg}^3 \text{ sec}}} \left[ \frac{1}{(633^\circ\text{K})^3} - \frac{1}{(803^\circ\text{K})^3} \right]$$

$$(88 \text{ cm}^2 \epsilon_R + 7.2 \text{ cm}^2) 420 \text{ sec} = \frac{+65 \text{ cm}^2 \text{ sec deg}^3}{4.062 \times 10^{-12}} \left( \frac{10^{-6}}{254} - \frac{10^{-6}}{518} \right)$$

$$36.9 \times 10^3 \epsilon_{\text{Rok}} + 3.002 \times 10^3 = (+16 \times 10^{12}) (+2 \times 10^{-9})$$

$$\epsilon_R = \frac{32}{36.9} - \frac{3.002}{36.9} = 0.787$$

$$\epsilon_R = 0.787 \text{ or } 0.79$$

The excellent agreement between the two values of Rokide emissivity arrived at by two different calculation routes indicates that either the approximate method or the exact method of emissivity calculation will give the correct result. A final computation may be conducted which eliminates the assumption that the emissivity of molybdenum is 0.2. Consider a "slab" of Rokided rod in the middle of the sample; compute the mass knowing the density and dimensions of the slab. This computation is within 0.5 percent since the sample was machined to within 0.3 mil tolerances. The analysis then proceeds in a manner similar to the exact solution, except that there is no term expressing heat loss from the unRokided portion of the sample. A value of 0.78 is obtained.

The "measured" Rokide emissivity value found in the present experiments is to be compared with the literature value of 0.85 to 0.93 for the total emissivity at 500°C and 1000°C, respectively. If the present Rokide "C" emissivity values are correct, an increase in radiator area of approximately 13 percent is required in practice to give the same heat rejection as that computed using the literature data for Rokide "C" emissivity.

#### 3.2.1.3 Rokide "C" Coated Molybdenum versus Rokide "C" Coated Copper

A copper rod, having dimensions similar to those of the molybdenum rod just described, was coated with Rokide "C", using the same process schedule and achieving the same coating thickness. The sample was instrumented with thermocouples, placed in a vac-ion pumped test chamber, and heated by electron bombardment to determine the Rokide-coating emissivity and stability for 500 hours of operation. Initial and final cool-down curves shown in Fig. 3-7 were analyzed in the same manner as just described for the Rokide-molybdenum curves. The value for Rokide "C" on copper is identical to that of Rokide "C" on molybdenum (i.e.,  $\epsilon \approx 0.78$ ).

No degradation of the coating on copper occurred over an extended test period of 500 hours operation at 600°C. The sample was rapidly thermal cycled some 30 times during test; however, no scaling, blistering, cracking, or peeling occurred. Moreover, the invariance of the cool-down curves over the 500-hour period attests to the coating stability. A slight haze, similar to that which appeared during the Rokide-molybdenum experiment, formed on the bell-jar surface, which resulted in a transmission loss of the same order.

To insure that the coating thickness of 2.5 to 3.0 mils was adequate for achieving the maximum emissivity value of Rokide "C", the molybdenum sample was stripped of thermocouples and resprayed using the same process schedule for an overall coating thickness of 7 mils. New couples were attached and the resulting

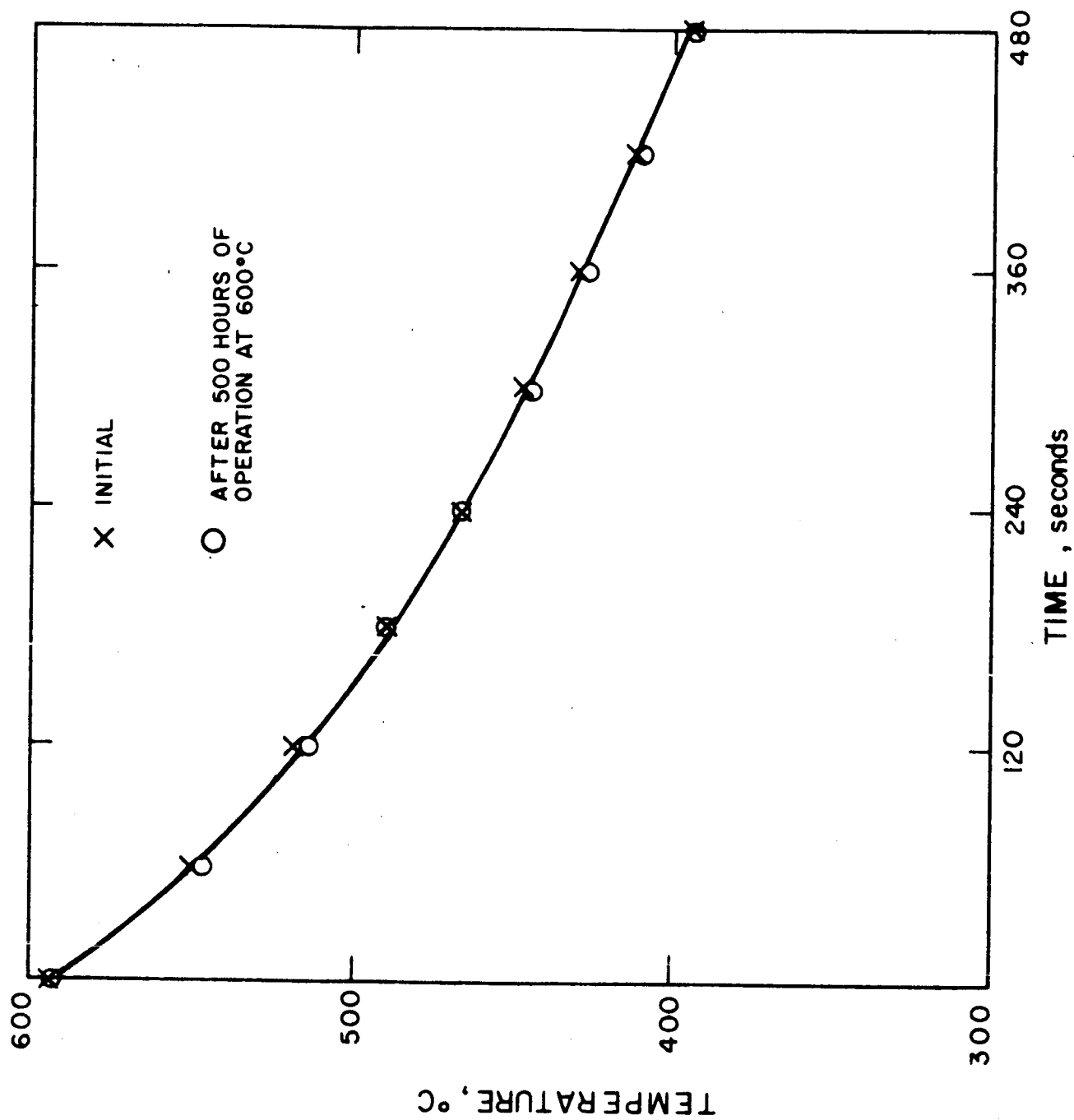


FIG. 3-7 COOLDOWN CURVES OF ROXIDE-COATED COPPER SAMPLE

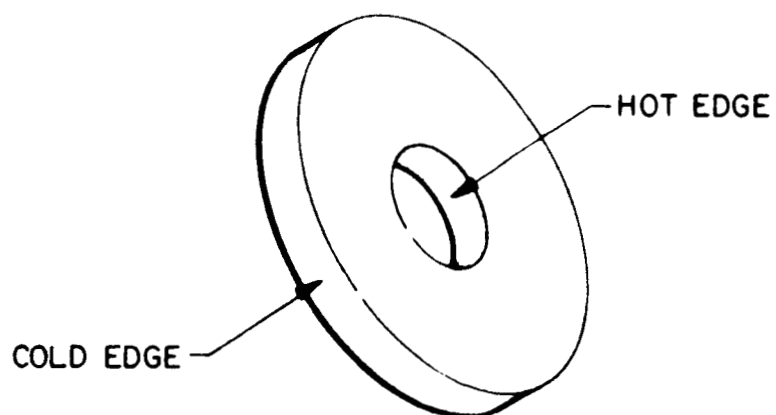
sample was operated again at 600°C. The identical nature of the coatings are best described as follows.

1. The identical sample temperature distribution was measured for the identical power input (filament plus bombardment).
2. An identical cool-down curve, point for point, was measured along the entire time axis.

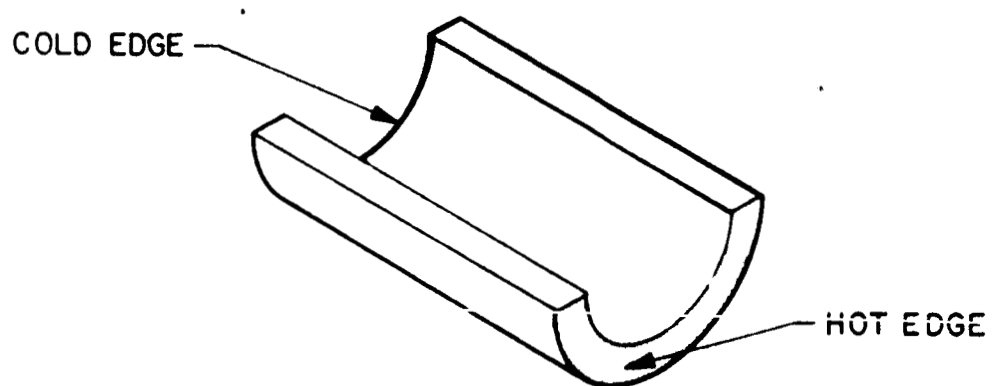
### 3.2.2 Radiator Fin Analysis

Several types of radiating fins have been used to reject heat from operating thermionic converters. Figure 3-8 displays some elementary forms of these radiators. The circular plate and cylindrical segment require major view-factor corrections either from the converter proper or the fin itself and for this reason are not given treatment in this study. For a selected material and weight limitation, the tapered plates of trapezoidal or triangular shape are the most efficient. It has been demonstrated (Refs. 3 and 4) that in convection media, the maximum heat rejection per unit weight occurs when the temperature gradient is linear along the length of the fin. MacKay indicates it is reasonable to extrapolate this to the case at hand, i.e., radiant heat transfer. Therefore, the following analysis is confined to the constant temperature-gradient fin which is physically tapered but in a nonuniform manner.

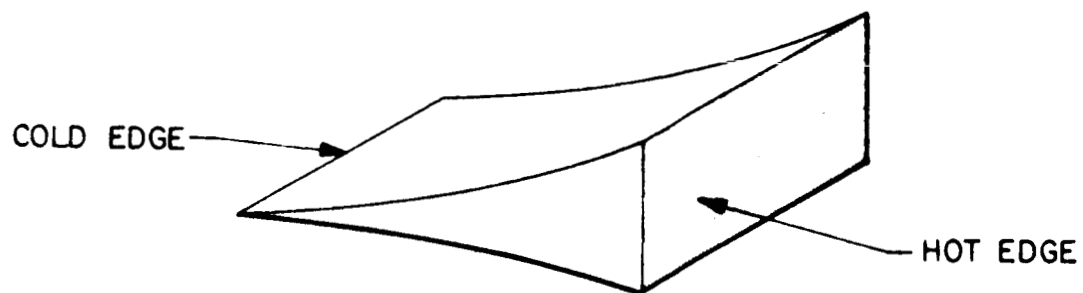
Figure 3-9 is a sketch of the dimensional relationships for the constant temperature-gradient fin. The assumptions in this analysis are: (1) the input heat to the fin is across the entire cross section of the hottest edge (2) the fin tip is zero thickness. In reality, the heat input from the collector to the radiator is concentrated at the center of the radiator's hottest edge which causes the heat flux lines to spread within the radiator. An analysis taking this into account would be extremely complex. Hence, it is approximated that heat input to the radiator is uniform across the hottest edge. The fin tip is obviously not zero in the practical configuration. In fact, some nominal thickness is desirable from a mechanical strength standpoint.



CIRCULAR PLATE FIN



CYLINDRICAL SEGMENT FIN



CONSTANT TEMPERATURE - GRADIENT FIN

FIG. 3-8 ELEMENTAL FORMS OF CONVERTER RADIATORS

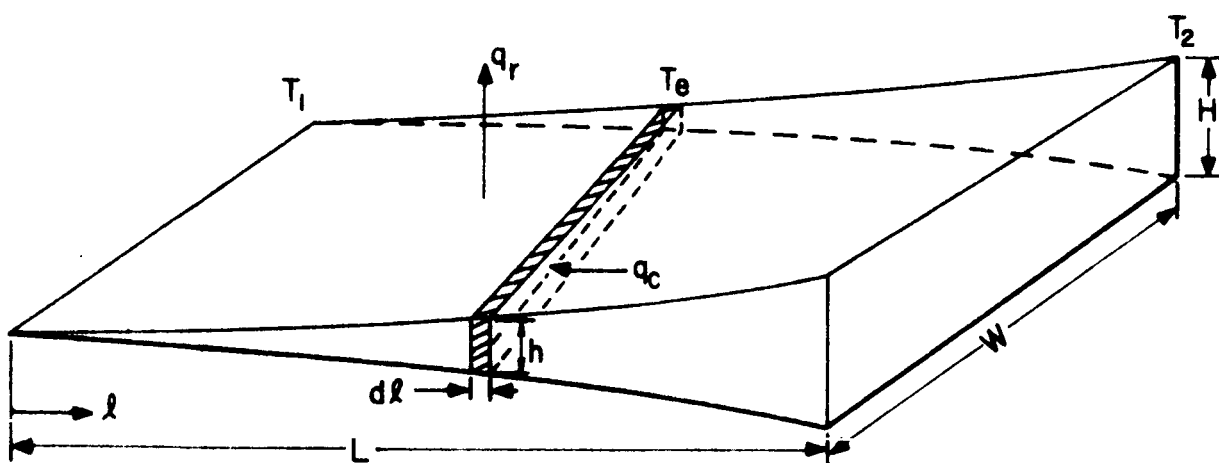


FIG. 3-9 MODEL FOR CONSTANT-TEMPERATURE-GRADIENT FIN ANALYSIS

Proceeding with the analysis, the amount of heat conducted through a section of the fin at right angles to the heat flux is:

$$q_c = - khW \frac{dT}{d\ell}$$

If a truly constant temperature gradient is required, then the temperature,  $T_e$ , at any selected element, may be obtained from the straight line equation,  $y = mx + b$ . Therefore,

$$T_e = \left( \frac{T_2 - T_1}{L - 0} \right) \ell + T_1 \quad (17)$$

where  $T_2$  is the temperature of the collector root,  $T_1$  is the temperature of the fin tip,  $L$  is the length from root to tip, and  $\ell$  is the position of the selected element. Differentiating this expression with respect to position yields

$$\frac{dT_e}{d\ell} = \frac{T_2 - T_1}{L} \quad (18)$$

which may be substituted into the heat flux equation:

$$q_c = - \frac{khW}{L} (T_2 - T_1) \quad (19)$$

The heat radiated from both sides of the fin between the elemental section and the tip is equal to this quantity, or,

$$-q_c = q_r$$

The heat lost from the elemental area in Fig. 3-6 is

$$dq_r = (2hd\ell + 2Wd\ell) \epsilon \sigma T_e^4 \quad (20)$$

where  $\epsilon$  is the emissivity of the radiating element and  $\sigma$  is the Stefan-Boltzmann constant.

Integrating the last expression over the surface area from the element under consideration to the fin tip and replacing  $d\ell$  by the functional relationship established between position and temperature,

$$q_r = \int_0^{q_r} dq = 2 \int_{T_1}^{T_e} \frac{(h + W) \sigma \epsilon L T_e^4}{T_2 - T_1} dT_e \quad (21)$$

The explicit functional relationship between  $h$  and  $T_e$  are not known; however, the heat lost from the area  $2hd\ell \ll 2Wd\ell$  and the calculation may proceed within 5 percent error.

$$q_r = 2 \left( \frac{T_e^5}{T_2 - T_1} - \frac{T_1^5}{T_2 - T_1} \right) \frac{W\sigma\epsilon L}{5}$$

since  $q_r = -q_c$

$$\frac{khW}{L} (T_2 - T_1) = \frac{2}{5} \sigma \epsilon L W \left( \frac{T_e^5}{T_2 - T_1} - \frac{T_1^5}{T_2 - T_1} \right)$$

Solving for the fin thickness:

$$h = \frac{\frac{2}{5} \sigma \epsilon L^2}{kW} \left[ \frac{T_e^5 - T_1^5}{(T_2 - T_1)^2} \right] \quad (22)$$

however, the element temperature  $T_e$  may be rewritten in terms of the boundary values  $T_2$ ,  $T_1$ ,  $L$  and the position variable,  $\ell$ ; so that the fin thickness,  $h$ , may be computed for a selected collector root and fin tip temperature at any given position along the fin. The final result after algebraic manipulation is:

$$h = \frac{\frac{2}{5} \sigma \epsilon L^2 \left\{ \left[ T_1 + \frac{\ell}{L} (T_2 - T_1) \right]^5 - T_1^5 \right\}}{k(T_2 - T_1)^2} \quad (23)$$

Applying this analysis to a problem of practical significance, assume that a forging die for a constant temperature-gradient radiator is to be designed along the lines of the EOS production converter. Assume further, that the radiator material is molybdenum with an emissive coating of Rokide ( $\epsilon = 0.78$ ) and that the approximate fin length and width dimensions are 2-1/4 inch by 2 inches. The collector root thickness is desired as a starting point for the die design. The following data is listed for the computation:

$$T_2 = T_{\text{coll. root}} = 600^{\circ}\text{C}$$

$$T_1 = T_{\text{fin tip}} = 520^{\circ}\text{C}$$

$L = 2\text{-}1/4$  inches, however the distance from the fin tip thermocouple to the collector root thermocouple is  $1\text{-}3/4$  inches.

$$l = \text{in this case} = L = 1\text{-}3/4 \text{ inches}$$

$$W = 2 \text{ inches}$$

$$\sigma = 5.67 \times 10^{-12} \text{ watts/cm}^2 \cdot ^{\circ}\text{K}^4$$

$$\epsilon = 0.78 \text{ (the emissivity of Rokide)}$$

$$k = 1.08 \text{ watts/cm}^2 \cdot ^{\circ}\text{K} \text{ (thermal conductivity of molybdenum in the temperature range of } 600^{\circ}\text{C)}$$

$$h = \frac{\frac{2}{5} \times 5.67 \times 10^{-12} \times 0.78 \times (1\text{-}3/4 \text{ in})^2 \times 6.45 \left\{ [793 + (80)]^5 - 793^5 \right\}}{1.07 (873 - 793)^2}$$

A dimensional analysis for  $h$  is as follows:

$$\frac{\frac{\text{watts}}{\text{cm}^2 \cdot ^{\circ}\text{K}^4} \times \text{in}^2 \times \frac{\text{cm}^2}{\text{in}^2} \times \frac{^{\circ}\text{K}^5}{^{\circ}\text{K}} \times \frac{\text{in}}{\text{in}}}{\frac{\text{watts}}{\text{cm} \cdot ^{\circ}\text{K}} \times \frac{\text{in}}{\text{in}} \times ^{\circ}\text{K}} = \frac{\text{watts}}{\frac{\text{watts}}{\text{cm}}} = \text{cm, the units}$$

(indicating that the final answer is dimensionally correct).

$$h = 0.99 \text{ cm or } 0.39 \text{ in}$$

The EOS production prototype converters measure 0.6 inch thick at the point where the collector root temperature is measured. The root, however, is not of constant thickness and tapers to  $1/4$  inch at the edge. The average thickness is near 0.45 inch, as compared to 0.39 inch via the analysis, which is good for a first order solution with the contingent assumptions listed at the beginning of the analysis.

Other relationships may be established from the analysis. For example, the heat transfer rate from the entire radiator is obtained by integrating the temperature over the limits of the hottest and coldest edges (i.e.,  $T_2$  and  $T_1$ ), so that

$$Q_r = 2 \int_{T_1}^{T_2} \frac{(h + W) \sigma \epsilon T_e^4 L}{T_2 - T_1} dT_e \quad (24)$$

where  $W \gg h$ , the integral is evaluated as

$$Q_r = \frac{2}{5} \sigma \epsilon L W \left( \frac{T_2^5 - T_1^5}{T_2 - T_1} \right) \quad (25)$$

Considering the production prototype converter, the heat radiated is slightly more than 100 watts. Add to this the electrical lead strap conduction of heat (copper braid or laminated copper straps) and the total of 120 watts is within 10 percent of the computed values of collector heat input for the production converter.

Finally, Eq. 25 may be simplified into a form that appeals to physical intuition by reducing the expression

$$\frac{T_2^5 - T_1^5}{T_2 - T_1}$$

to one of  $T^4$  dependence plus lower order polynomials.  $Q_r$  then reverts to the familiar Stephen radiation law with an assortment of terms accounting for the constant-temperature gradient of the fin which reduces the overall heat transfer rate from that of a constant temperature plate.

### 3.2.3 Non-Integral Collector-Radiator

The EOS production prototype converter contains an integral collector-radiator which is die forged from molybdenum bar stock. The major advantages of the molybdenum integral collector-radiator are: (1) a continuous heat transfer path unimpaired by any

brazed interface or thermal impedances (2) a mass-production technique for fabrication, and (3) a mechanically strong high-temperature structural member. The disadvantage is lower specific performance since other materials, such as copper, due to their higher thermal conductivity lead to reduced weight for equivalent converter thermal power transfer.

An investigation has been initiated which will study the problems of reliably bonding a molybdenum collector to a copper radiator for use under thermal cycling conditions. The parts shown in Fig. 3-10 were selected to evaluate a brazed joint design which captures the copper radiating fin so that the thermal expansion mismatch keeps the parts in compression. Shim-stock Nicro brazing material (82 percent gold - 18 percent nickel) 0.002 inch thick was inserted in the slot on either side of the copper. Nicro wire (of 0.030 inch diameter) was placed at the copper-molybdenum intersection on either side of the fin. The assembly was vacuum brazed at 925°C, the melting point of Nicro. This resulted in a brazed fillet that contained no voids or cracks. As indicated in the sketch, the assembly is nominally converter size to permit simulation of thermal fluxes through the bonded area on the order of 200 to 250 watts. Over 100 cm<sup>2</sup> of copper radiator will be provided to provide ample heat dissipation for the experiment. The molybdenum portion of the assembly is an integrally forged part in which the mounting holes and brazed joint are machined.

The assembly will be mounted in a vacuum bell jar and heated indirectly at the collector end by electron bombardment. Thermocouples will be attached to either side of the brazed interface to measure the temperature drop across the joint for various thermal loads.

After determining the initial thermal characteristics of the assembly, it will be subjected to at least 100 thermal cycles and re-evaluated. The upper limit of the cycle will be 600°C (a common collector root temperature), and the lower limit of the cycle will be 200°C, since the time to reach lower temperatures by radiation cooling

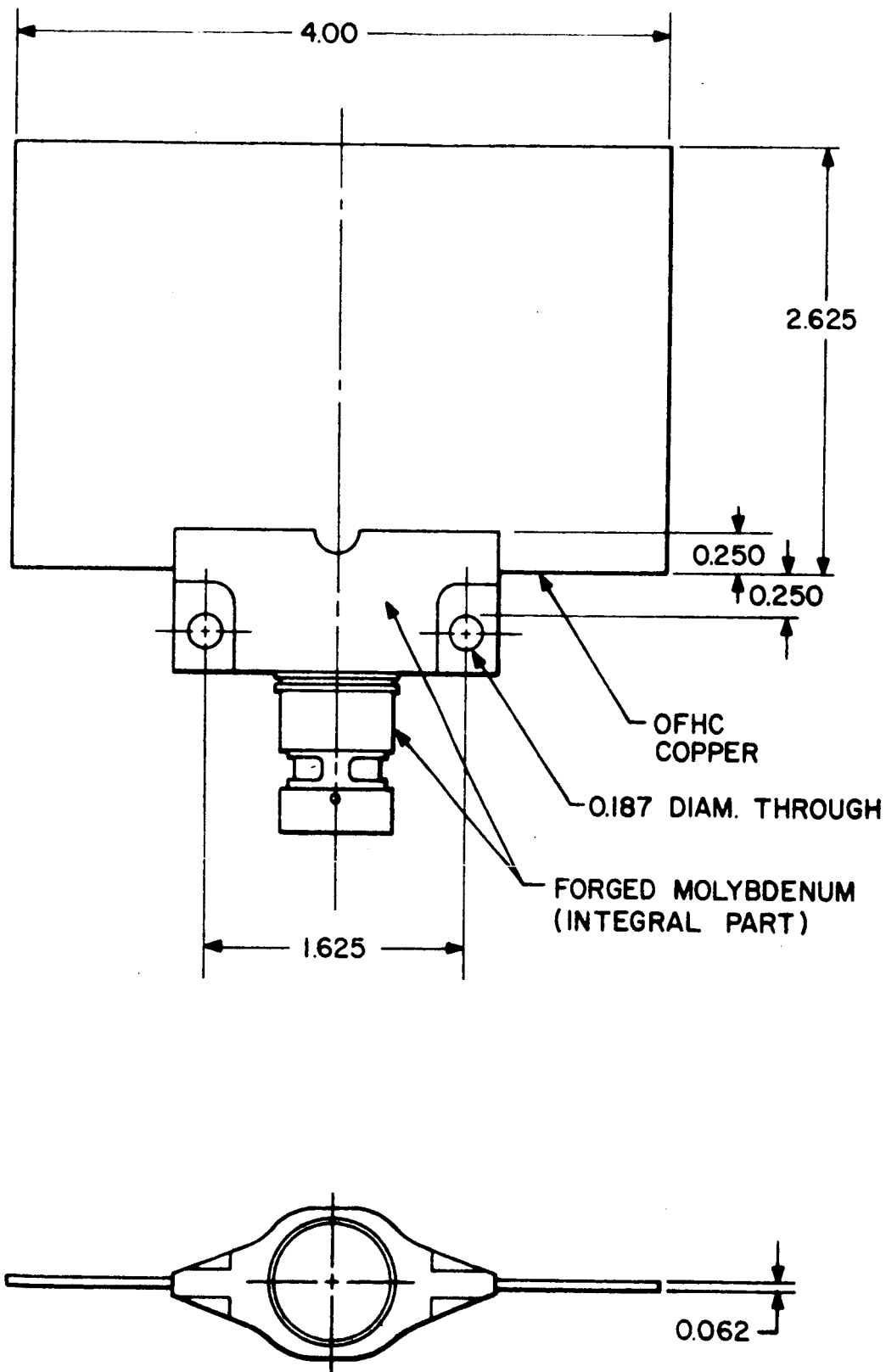


FIG. 3-10 NONINTEGRAL COLLECTOR-RADIATOR ASSEMBLY

becomes excessive. The cycling test should also provide a further evaluation of the Rokide-copper system under severe thermal cycling conditions.

The thermal expansion mismatch between molybdenum and copper in the temperature range of  $600^{\circ}\text{C}$  is severe. However, the joint geometry purposely encapsulates the higher expansion member (copper) with the lower expansion member (molybdenum). This scheme appeared to provide a good bonding in the composite collector geometry and should produce similar results for this application although there is no expansion constraint on the copper along the fin top.

After the test is concluded, the bond between the copper and molybdenum will be metallurgically examined.

### 3.3 Converter Fabrication Investigation

#### 3.3.1 High-Temperature Brazing

In high-performance converters, there are two types of materials joining that require special consideration. The first is bonding rhenium wafers or sheet stock to a molybdenum substrate to obtain economically a low-cesiated-work-function collector surface. The second is bonding a rhenium envelope (welded to a rhenium emitter) to the niobium sealing flange and emitter lead strap to form a minimum-resistance electrical path while retaining vacuum integrity through thermal cycling. Both bonds are located in regions of a thermionic converter that operate over  $700^{\circ}\text{C}$  (especially the collector) and in a cesium vapor environment of from 3 to 15 mm Hg, which severely limits the choice of braze materials. Moreover, rhenium forms either low-melting-point eutectics or brittle inter-metallic compounds with most materials. High-purity (99.9 percent) vanadium was selected as a braze material to investigate the joining of rhenium to materials such as niobium and molybdenum. Vanadium displays no low-melting-point eutectic in the rhenium system and takes only a moderate amount of rhenium into solution at melt; hence, it retains reasonable ductility.

Two sample assemblies of rhenium and niobium have been vacuum brazed with 99.9 percent pure vanadium to establish the materials and conditions necessary for affecting a ductile joint between rhenium envelopes and niobium sealing flanges. Both assemblies were brazed in susceptor-can environments at  $1 \times 10^{-6}$  mm Hg. One assembly was brazed for 3 minutes at  $1900^{\circ}\text{C}$ , the melting point of vanadium. The other assembly was brazed for 3 minutes at  $2150^{\circ}\text{C}$  to examine the effect, if any, of overbrazing. Figure 3-11 is a microphotograph of the vanadium overbrazed showing evidence of an undesirable void structure in the vanadium and the formation of a vanadium-rhenium interface. Figure 3-12 is a detail of this interface which was traversed with a micro-hardness tester and was found to have a hardness value of greater than Rockwell "C" 60 as compared to a Rockwell "C" 27 for the rhenium. This degree of hardness suggests the formation of an intermetallic compound at the vanadium-rhenium interface. Figure 3-13 is a microphotograph of the vanadium braze at  $1900^{\circ}\text{C}$ , which has no void structure or evidence of intermetallic formation. In addition, the hardness value of the braze area is 20 Rockwell units less than the overbrazed sample. Both samples indicate a high-quality bond at the niobium interface, which agrees with metallurgical information that a continuous series of solid solutions are formed from the melting point of vanadium to the melting point of niobium ( $2415^{\circ}\text{C}$ ).

Vanadium would, therefore, appear to be a satisfactory braze material for bonding rhenium to niobium. Its use would apparently result in minimum void structure for good electrical conduction and heat transfer, as well as reasonable ductility to support thermal cycling.

### 3.3.2 Heater-Wire End Seals

Repeated difficulty has been experienced in the connection of electrical leads to the common variety of sheathed heater wire used to supply heat to the cesium reservoir and radiator spade. The sheathed heaters (usually tantalum, alumina, and tantalum center

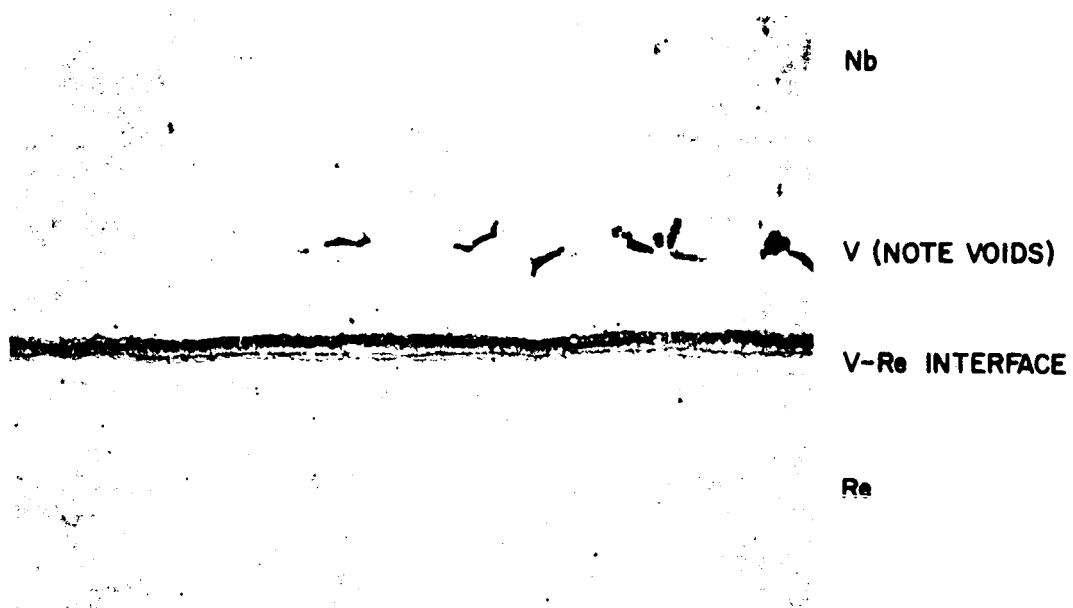


FIG. 3-11 VANADIUM OVERBRAZE AT 2150°C OF  
RHENIUM TO NIOBIUM (X500)

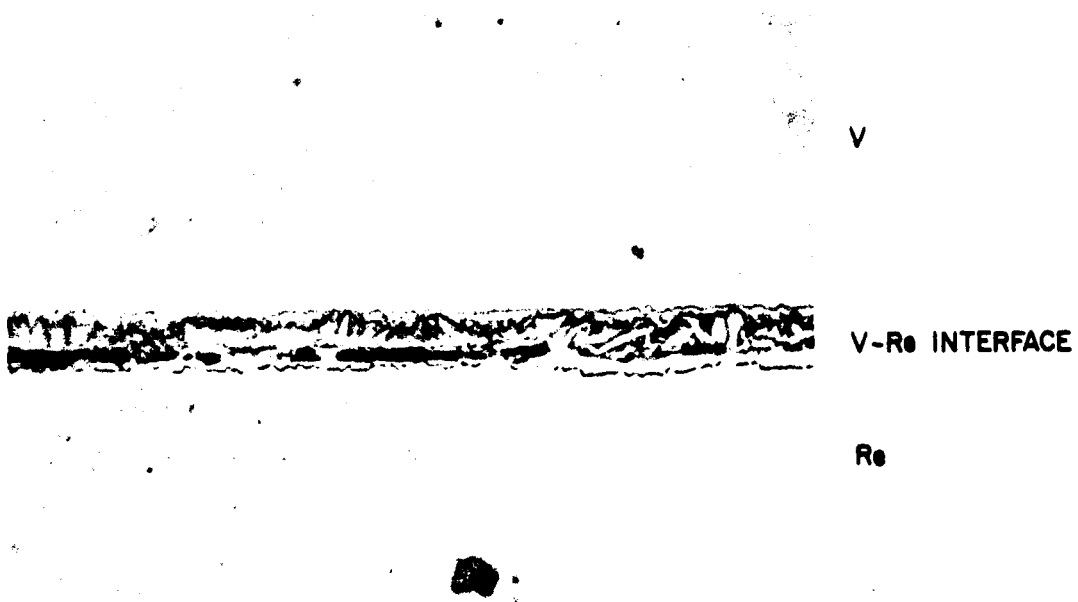


FIG. 3-12 DETAIL OF OVERBRAZED VANADIUM-RHENIUM  
INTERFACE (X1000)

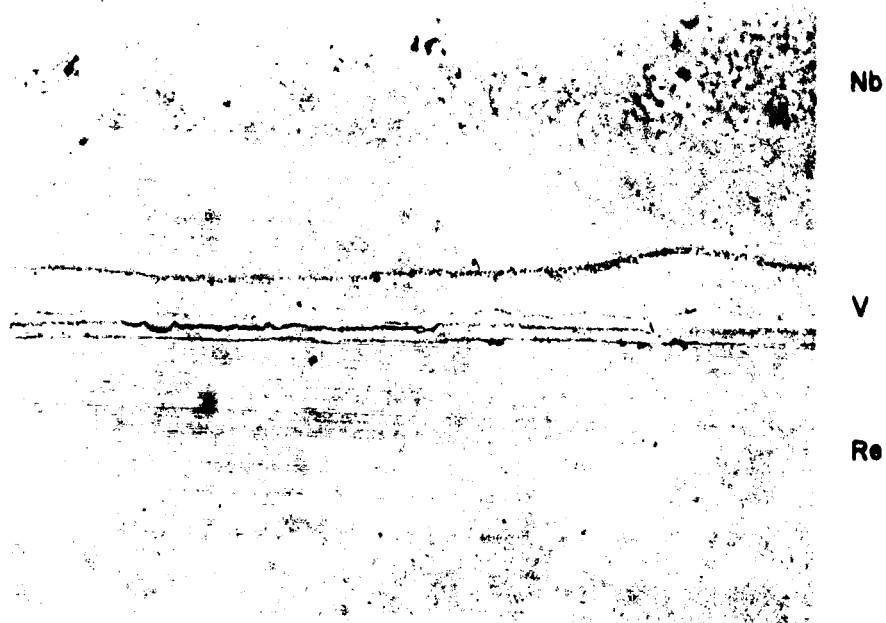


FIG. 3-13 VANADIUM BRAZE AT 1900°C OF RHENIUM  
TO NIOBIUM (X500)

conductor) are claimed to be capable of electrical inputs of 50 - 100 watts/linear inch. The problem is to efficiently transfer 10-20 amperes by mechanical attachment to a 0.060-inch-diameter center conductor. Furthermore, there must be good heat transfer from the area of connection; otherwise, the end of the center conductor operates at temperatures which are too high and may fail due to excessive interaction with the alumina insulation.

Figure 3-14 is a sketch of the sheathed heater wire, a hollow feedthrough, and copper inserts assembled prior to fabrication. A heavy-duty, stake-on tool is employed to mechanically bond the feedthrough to the copper inserts. This mechanical bond was evaluated by attaching two feedthroughs to a brazed heater wire assembly on a converter radiator and passing 15 amperes through the assembly for a period of 100 hours. The end seals were then subjected to 200 cycles of peak current load at 20 amperes with a voltage drop of 6.2 volts across the end-seal connections. The heater wire and end seal remained operative without disconnection, burnthrough, or degradation of any type. The testing of this assembly represents a far more severe case than would be encountered in converter performance tests, and the results, therefore, should apply to converters without difficulty.

### 3.3.3 Converter Seal-Off

Figure 3-15 is an example of a marginal converter seal-off of the reservoir tubulation. The seal-off is made by the application of a local pressure sufficient in magnitude to cold-weld a copper tube. Prepressure is applied with an instrument known as a pinch-off tool. The cold-weld in Fig. 3-15 is leak tight and has the external appearance of being a good pinch-off. In micro-section, however, the minimum seal thickness is found to be only 0.0006 inch. A pinch-off such as this is highly unreliable under any pressure differential between the device and its environment. Moreover, it cannot suffer accidental damage without loss of the converter.

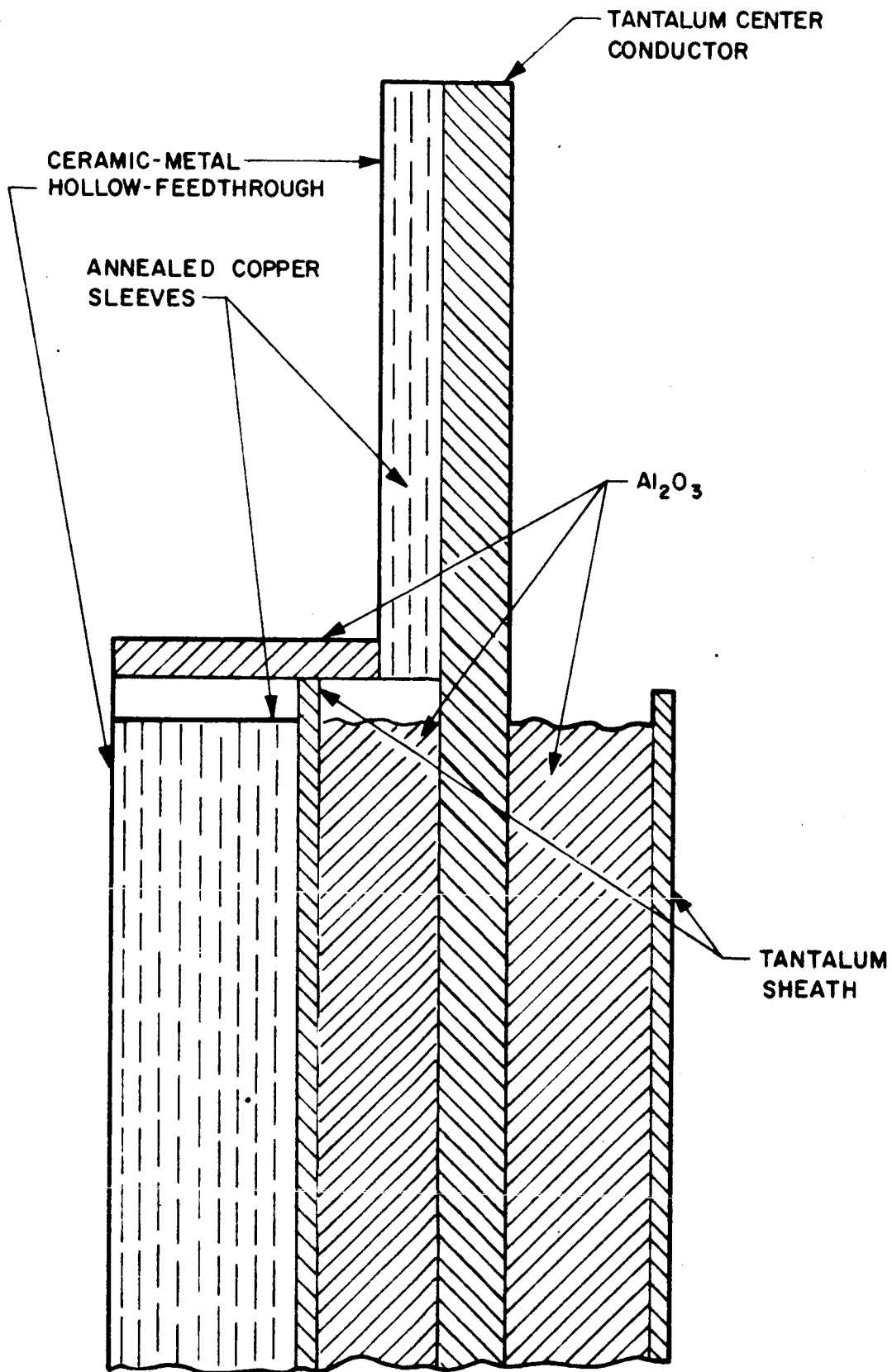
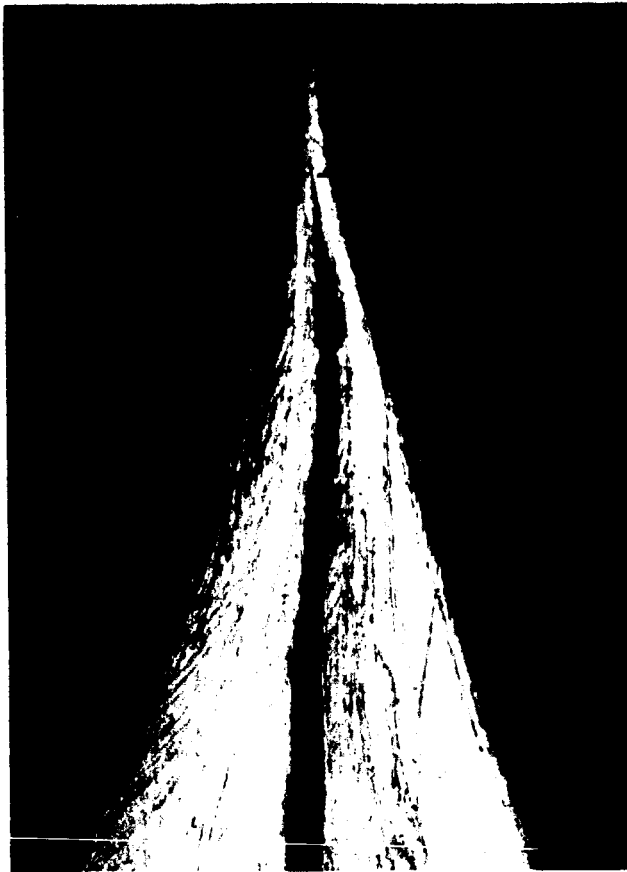


FIG. 3-14 END CONNECTION FOR SHEATHED HEATER WIRE



0.0006 in. MINIMUM  
SEAL THICKNESS

FIG. 3-15 MARGINAL PINCHOFF OF COPPER  
TUBING RESERVOIR (X100)

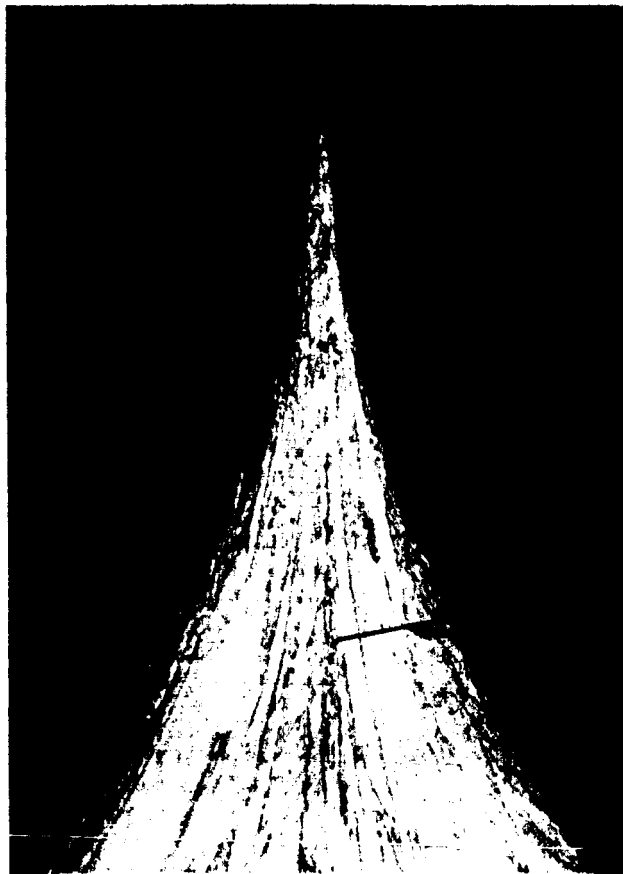
An identical length of copper tubing was processed in an identical manner, vacuum annealed at the same schedule and pinched off with the same pinch-off tool. The resultant seal is shown in Fig. 3-16, where a minimum seal thickness of 0.007 inch is indicated. The pinch-off tool used was a hand pinch-off tool which has the physical appearance of a bolt cutter and requires continuous and delicate adjustment with no reasonable assurance that any selected adjustment will yield a satisfactory pinch-off.

Another type of pinch-off tool is the hydraulic-actuated tool, which encases the pinch-off rollers or jaws in machined guides. With less adjustment and a consistent stroke before the weld, the hydraulic tool appears to produce more satisfactory welds. A group of ten pinch-offs made with a Kane hydraulic tool will be examined for consistency of seal thickness.

#### 3.3.4 Ceramic-Metal Seals

An investigation is being conducted to determine the long-life reliability, thermal-shock resistance, and fabrication parameters of a nickel-zirconium active alloy braze of high-purity alumina-to-niobium flange members. Of particular interest to this investigation, is the maximum flange thickness that can be brazed to a selected alumina ceramic thickness without sacrifice in yield or reliability. Previous EOS converters were fabricated with metal flanges 0.010 inch thick. These provided sufficient yield during fabrication but required "positive-type" spacing of the interelectrode gap to prevent flange flexure from setting an inconsistent interelectrode spacing. Since the first design iteration of the high-performance converters built on this program is excluding the positive-type spacing, thicker flange members are being sought to avoid "spacing" in the seal structure.

Twenty and 30 mil niobium sheet stock is being spun for this study. Completed flanges will be brazed to AL 995 (Wesgo) ceramics, welded to refractory electrodes of tantalum, loaded with cesium, and sealed off. Figure 3-17 is a sketch of this device in an



0.007 in MINIMUM  
SEAL THICKNESS

FIG. 3-16 SATISFACTORY PINCHOFF OF  
COPPER TUBING SAMPLE (X100)

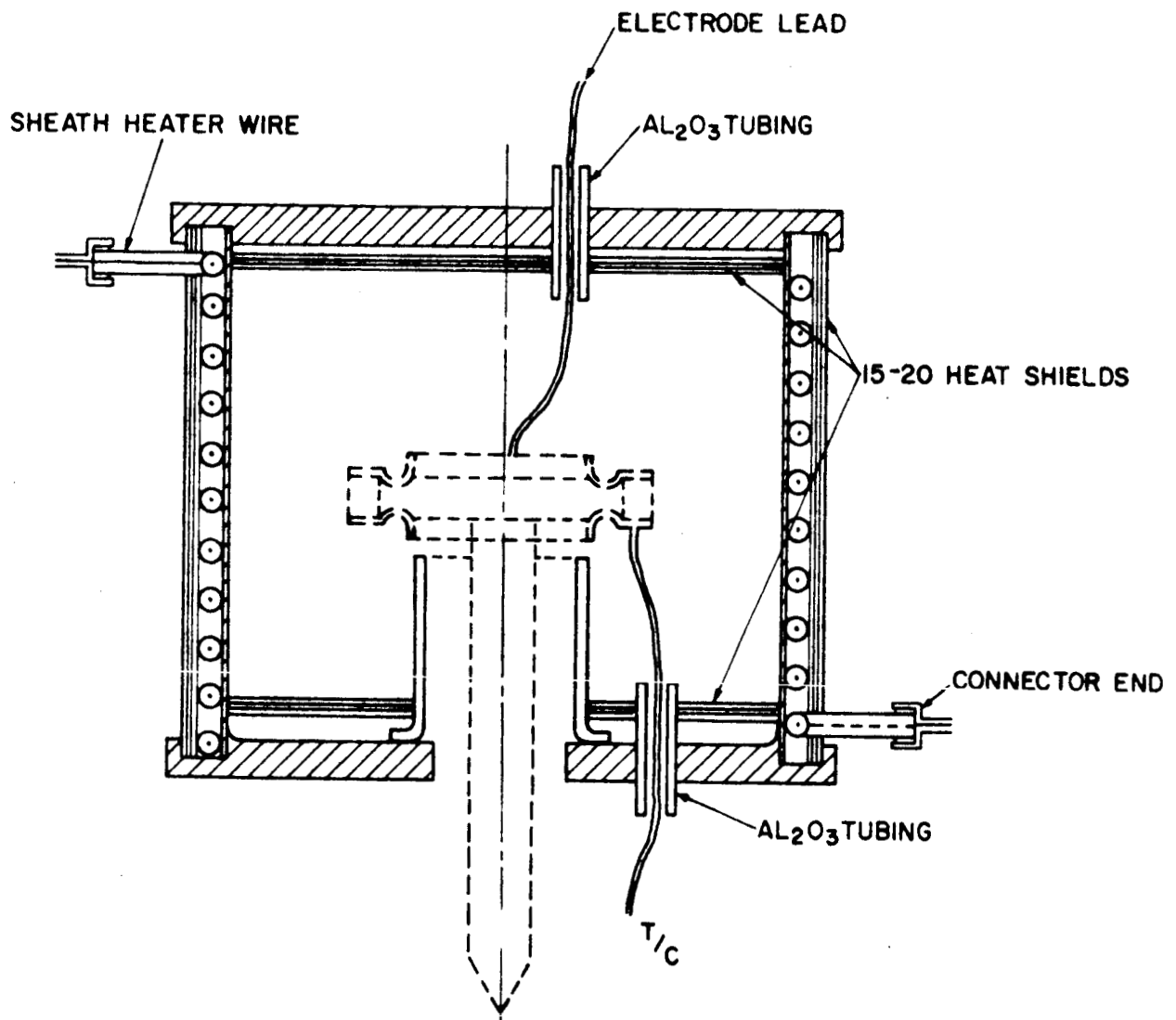


FIG. 3-17 THERMAL ENVIRONMENT OVEN FOR CERAMIC-METAL SEAL TESTING

environment oven which is designed and built to thermally test the seals. The oven has been completed and operated with only a  $4^{\circ}\text{C}$  temperature differential from top to bottom and from side to side. The oven is capable of operation in excess of a  $1000^{\circ}\text{C}$ , if necessary. The seal testing temperature has been selected at  $600^{\circ}\text{C}$  (although some tests may be made at  $700^{\circ}\text{C}$ ). The cycle temperature for investigating thermal shock is from  $600^{\circ}\text{C}$  (or  $700^{\circ}\text{C}$ ) to  $250^{\circ}\text{C}$  in a 15 minute time interval.

### 3.3.5 Interelectrode Spacing

A study has been initiated to take direct measurements of the interelectrode spacing in a thermal mock-up of a thermionic converter. The interelectrode spacing has been calculated by computing the thermal expansion of the electrodes and has been measured indirectly by way of cesium conduction data. Both methods yield useful information but lack the required accuracy ( $\pm 0.0001$  inch) and absolute reference that only direct optical measurement can supply. Figure 3-18 is a conceptual setup of a means to allow a direct microscopic measurement of the spacing between electrodes in a simulated converter.

The interelectrode spacing of a converter is a result of thermal expansion differences between the emitter support structure (envelope) and the collector. The mock-up device in Fig. 3-18 will be operated over the range of emitter and collector temperatures encountered during converter operation. The collector temperature will be measured at a distance of 0.050 inch from the surface by means of an immersion thermocouple and directly at the collector root to insure the correct temperature difference. A sheathed heater wire is brazed to the collector to insure that the proper thermal loads are sustained during measurement. The temperature of the emitter lead straps and sealing flanges also will be measured to maintain the proper  $\Delta T$  between the emitter and emitter leads (or seals). The expansion of both electrodes will simulate converter operation and the interelectrode spacing will be measured directly through a small viewing slit in the envelope. More

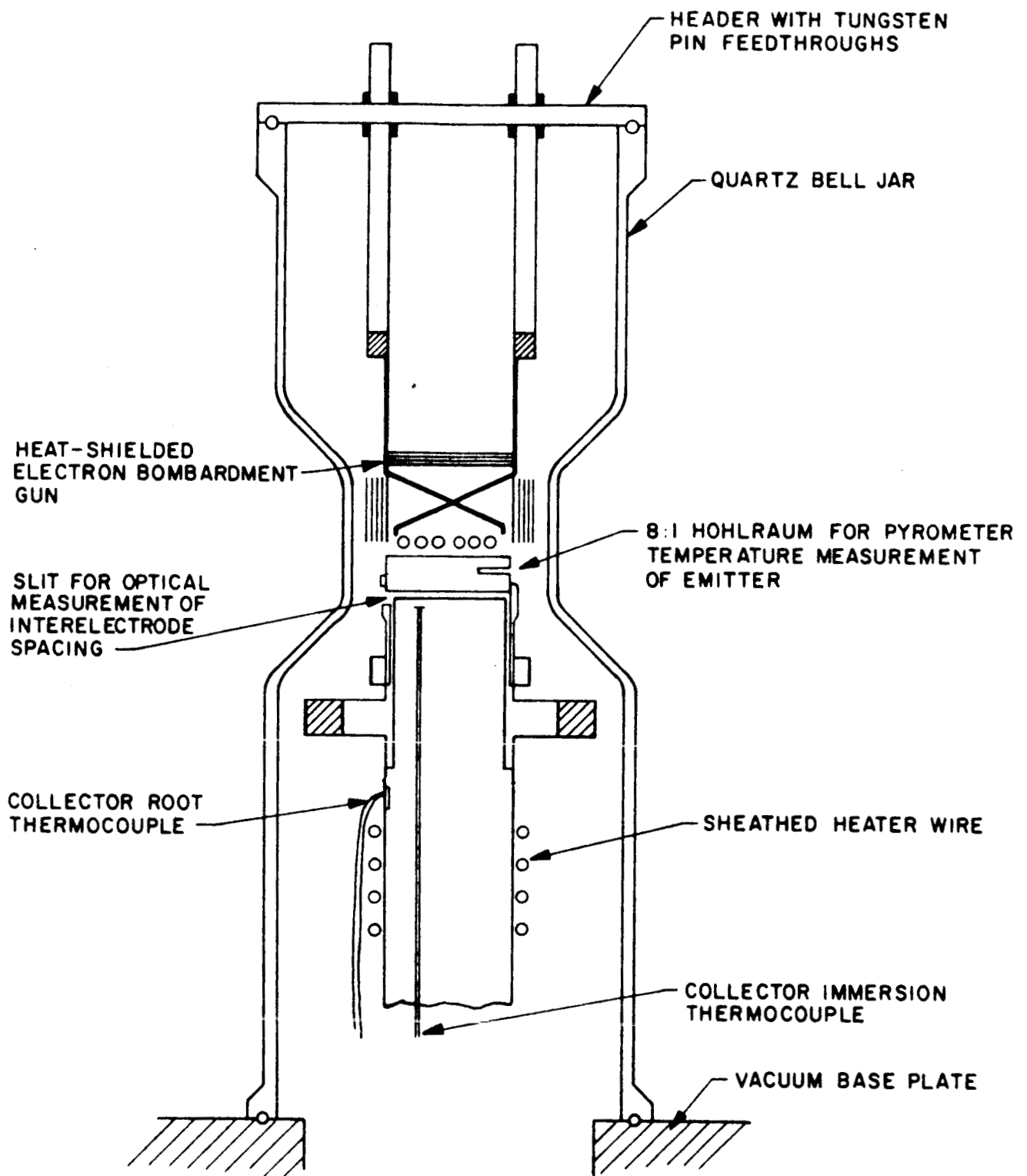


FIG. 3-18 SETUP FOR MEASURING INTERELECTRODE SPACINGS IN A MOCKUP CONVERTER

than one slit is planned so that a measure of the parallelism of the electrodes can be achieved.

Optical measurements of the spacing will be taken for various collector heat loads and emitter temperatures that are pertinent to converter operation.

#### 4. CONVERTER DESIGN

A converter design effort has been recently started to design high performance converters with the following characteristics:

1. A converter efficiency greater than fourteen percent at an output voltage of 0.8 volts and a true emitter temperature of 1735°C. The efficiency is defined as: the electrical power output divided by the total bombardment power, excluding the filament power used to heat a .020" filament wire.
2. A converter power density of 20 watts/cm<sup>2</sup> at an output voltage of 0.8 volts and a true emitter temperature of 1735°C. The total emitter area is two (2.0) cm<sup>2</sup>.
3. The weight of each converter consistent with achieving a four-converter generator weighing 4 pounds.

As part of the design effort, each converter fabricated during the program will be designed in an iterative fashion with inputs from the secondary experiments, data from the variable parameter vehicle, and performance from previously tested converters.

As a design starting point, the trade-off between mechanical rigidity (derived from a spacing ring which connects the envelope to the collector) and the achievement of higher performance through the achievement of lower interelectrode spacing. The retaining ring, utilized in EOS production converters, also provided consistent spacing from device to device but there was speculation that the value may have been too large for the achievement of power densities in excess of 20 watts/cm<sup>2</sup> at 0.7 volt and 2000°K emitter temperature.

The ceramic metal seal and interelectrode spacing investigations will be completed or near completion this next quarter.

#### 5.6 Converter Design

The design of high performance thermionic converter will be completed for J.P.L. approval. Subsequent design iterations will proceed during the fabrication and test of individual converters.

## 5. PROGRAM FOR NEXT QUARTER

### 5.1 Variable Parameter Test Vehicle

The variable parameter test vehicle will be fabricated in the next quarter. Upon completion, the first set of electrode materials will be tested for power output, emission and work function values and variation of power output as a function of interelectrode spacing.

### 5.2 Emitter Materials Process Study

The complete process schedule for tantalum and rhenium electrodes will be completed. The process schedules should result in the achievement of uncontaminated and stable emitter surfaces which do not change characteristics with time at temperature.

### 5.3 Non-Integral Collector Radiator

Various geometries and braze materials bonding molybdenum to copper will be examined, during the next quarter to improve radiator heat rejection vs weight. The thermal impedance of the bond joint and reliability of this joint during thermal cycling will be examined.

### 5.4 Composite and Non-Composite Collector Experiments

The composite and non-composite collector experiments will continue during the next quarter. The temperature drop of selected collector structures will be measured as a function of thermal fluxes ranging from 100-250 watts.

### 5.5 Converter Fabrication Investigations

The heater wire end seal, converter seal-off, high temperature brazing and electron beam welding investigation will be completed.

#### REFERENCES

1. D. B. MacKay, "Radiant Heat Transfer from Tapered Fins," a paper presented to the American Institute of Chemical Engineers, August 1960, Buffalo, New York.
2. T. E. Waterman and H. J. Hirschhorn, "Handbook of Thermophysical Properties of Solid Materials," MacMillan, New York 1961.
3. G. E. Alves, "Co-Current Liquid Gas Flow in a Pipe-Line Contractor," Chemical Engineering Progress Vol 50, 1954 p. 449
4. W. L. Badger, "How a Long-Tube Evaporator Works," Chemical and Metallurgical Engineering, Vol. 46, 1939, p. 640
5. Technical Report AFAPL-TR-65-7, January 31, 1965.

APPENDIX A  
PROCEDURE FOR CHEMICAL CLEANING OF TANTALUM

I. DESCRIPTION

The following procedure describes a method for chemically cleaning tantalum prior to vacuum outgassing.

II. EQUIPMENT LIST

1. Beakers of assorted sizes.
2. Hot plate.
3. Ultrasonic cleaner (minimum of 60 watts average power).
4. Bunsen burner, stand, and hot pad.
5. Forceps of assorted sizes.
6. Lint-free and sulphur-free paper.
7. Distilled water.
8. Ethyl alcohol ( $C_2H_5OH$ ).
9. Hydrochloric acid (HCL), 37 percent.
10. Chromic acid (saturated solution of chromium trioxide).
11. Sulphuric acid ( $H_2SO_4$ ), 96 percent.
12. Stiring rod
13. Graduate
14. Balance, triple beam  $\pm 0.1$  gram
15. Glass storage container, 1 gallon

III. SAFETY PROCEDURE FOR PREPARATION OF CHROMIC ACID

All materials are corrosive. Avoid spilling. In case of spillage, wash away immediately with large quantities of water.

Sulfuric acid releases a large amount of heat when mixed with water. Therefore, use caution and follow instructions exactly. Add acid to water.

The following safety apparatus must be used while preparing the solution:

1. Rubber gloves
2. Goggles or face mask
3. Full length rubber or plastic apron

#### IV. PREPARATION OF SATURATED CHROMIC ACID

##### 1. Materials

- a. Chromium trioxide (chromic acid), solid, technical grade
- b. Sulfuric acid, concentrated, 96 percent, ACS specification
- c. Distilled water

##### 2. Equipment

- a. Graduate (1 liter)
- b. Beaker (4 liters)
- c. Stirring rod
- d. Balance, triple beam,  $\pm 0.1$  gram
- e. Glass storage container, 1 gallon

##### 3. Procedure

- a. Measure 2 liters of distilled water into beaker.
- b. Add chromium trioxide and stir until solution is saturated.
- c. Slowly and while stirring, carefully add 1100 ml of concentrated sulfuric acid.
- d. Store in glass bottle, label "saturated chromic acid solution."

#### NOTE

Solution should be discarded if it shows a greenish cast. There may be legal restrictions on the disposal of chromate solutions.

#### V. SAFETY PROCEDURES FOR CLEANING PROCESS

All materials are corrosive. Avoid spilling. In case of spillage, wash away immediately with large quantities of water.

The following are mandatory while cleaning parts with acid solutions:

1. Rubber gloves
2. Goggles or face mask
3. Rubber or plastic apron

## VI. CLEANING PROCEDURE

### 1. Materials

- a. Ethyl alcohol ( $C_2H_5OH$ )
- b. Hydrochloric acid (HCL), 37 percent
- c. Chromic acid solution
- d. Distilled water
- e. Hot plate
- f. Ultrasonic cleaner (minimum of 60 watts average power)
- g. Lint-free and sulphur-free paper
- h. Beakers of assorted sizes

### 2. Procedure

- a. Place part to be cleaned in beaker of ethyl alcohol. Place beaker in ultrasonic cleaner. Clean for approximately 60 seconds.
- b. Remove parts from ethyl alcohol - allow to dry.
- c. Place parts in beaker of boiling hydrochloric acid for approximately 30 seconds
- d. Remove from hydrochloric acid and rinse in beaker of boiling, distilled water for approximately 2 minutes.
- e. Remove from distilled water - allow to dry.
- f. Dip in ethyl alcohol - remove and allow to dry.
- g. Place parts in beaker of hot chromic acid ( $110^{\circ}C$ ).
- h. Remove from chromic acid and rinse vigorously in large beaker of cold, distilled water.
- i. Rinse parts in boiling, distilled water for approximately 2 minutes.
- j. Rinse parts in cold, distilled water for approximately 10 seconds.
- k. Remove parts from distilled water - allow to dry.
- l. Rinse parts in clean, ethyl alcohol - remove and dry with hot air blast.

- m. Visually inspect each part for contamination such as fingerprints, water stains, and discoloration. Parts must be free of any such contamination. PRESENCE OF ANY CONTAMINANTS DICTATES THE NEED FOR AN ENTIRE REPROCESSING OF THE AFFECTED PART.
- n. Wrap parts in lint-free, sulphur-free paper.
- o. Seal in polyethylene bag.